UNIVERSITÀ DEGLI STUDI DI PADOVA

Dipartimento di Fisica e Astronomia "Galileo Galilei"

Corso di Laurea Magistrale in Fisica

Tesi di Laurea

Perturbations of two planets on the dust component of a circumstellar disk

Relatore	Laureando
Prof. Francesco Marzari	Andrea Marangoni

Anno Accademico 2018/2019

Contents

Chapter 1

Introduction

The question about the formation of planets has arisen since a long time, when the only known planetary system was the Solar System.

In this respect, the first attempt of a theory had been made by the French philosopher Descartes in 1644, even if it was mostly based on philosophical assumptions, rather than on scientific ones [1], [2].

In his work, Descartes hypothesized that Earth and the other planets had formed from some vortices around the primitive Sun.

In 1796 Laplace, starting from Swedenborg's idea, proposed in his treatise *Exposition du system du monde* the nebular model for the formation of planets around the Sun [3].

In this model, an initial approximately spherical and dusty cloud, surrounding the central star, is slowly rotating. As time passes, the nebula cools and collapses, creating a disk-like structure that spins faster around the Sun in order to conserve angular momentum. During the collapse, the nebula threw off some gaseous and dusty material, which is arranged in annular rings. These rings would have been the birthplaces for planets, formed by condensation of gas and dust.

The same process, on a smaller scale, where the star was replaced by the planet, could also explain satellites formation.

The main problem of this model was the Angular Momentum Problem. This issue refers to the fact that although the Sun contains the 99% of the mass of the Solar System, it is responsible only for the 1% of the angular momentum. Indeed, the greatest part of the Solar System's angular momentum comes from giant planets.

During the twentieth century various theories and models were proposed, all concerned with the solution of this problem.

In 1944 the model proposed by von Weizsäcker took up Descartes' idea, supposing that planets had formed in a turbulent, viscous disk around the Sun by particle accretion.

The main contribution of this model was to introduce the concept of angular momentum transport due, in this case, to viscosity.

Few years later, Hoyle introduced magnetic braking in order to give a better explanation for the transfer of angular momentum from Sun to the disk material.

This model is based on a circumstellar disk, characterized by the presence of a gap between the inner edge of the disk and the star. The presence of magnetic field lines filling the gap allows the transport of angular momentum from Sun to the disk.

Angular momentum transfer through magnetic field is more efficient than the transfer due to viscosity. Indeed, von Weizsäcker model required the contact between Sun and the orbiting material in order to have transport of angular momentum through hydrodynamic effects.

The thought that Solar System was nothing but one out of thousands of planetary systems was definitely validated in 1990s, when the first detections and confirmations of exoplanets, among which the detection of the first exoplanet orbiting a Solar-type star in 1995, awarded with Nobel Prize to Mayor and Queloz in 2019, paved the way to the possibility of testing all these theories through the comparison with other planetary systems.

Nowadays, the growing number of missions dedicated to the search and analysis of exoplanetary systems have brought to the discovery of more than 4000 planets [4].

All these discoveries allowed to answer certain questions, but gave rise to other issues.

Various methods and techniques to detect protoplanetary disks around stars have been developed during these years. Such methods include

- Detection of infrared excesses over the stellar photospheric flux, that indicate the presence of warm dust surrounding the star within 1 AU.
- H_α emission lines (and other emission lines) and ultraviolet excesses, indicating the accretion of gas onto the star.
- Detection of millimeter or sub-millimeter flux, signaling the presence of cool dust in the outer disk regions.
- Disk imaging

Instruments like ALMA [5] (Atacama Large Millimeter/submillimeter Array), formed by 64 12 m antennas which probe the sky in the portion of radio waves, and SPHERE [6], an extreme adaptive optics system and coronagraphic facility at the VLT, are providing us with data and observations of circumstellar disks and, among other things, allow us to study the dust component of these disks.

And it is just thanks to VLT/SPHERE that, in 2018, astronomers made the first robust detection of a forming planet within a gap in a circumstellar disk (Fig. 1.1) [7].

Other observations of possible planet candidates into protoplanetary disks had been made in the past years, but most of them were suspected to be disk features.

The detected planet, called PDS 70b, is a giant planet, with a mass few times Jupiter mass, and it is located at about 20 AU from the central star.

Any theory oriented to explain planet formation must account for the data and observations both from Solar System and from exoplanetary systems.

In particular, a good working theory for planet origin has to clarify various features, such as [8]:

- Orbital features of the Solar System, in particular the fact that planets have nearly coplanar orbits, lying on Sun's equatorial plane, and the fact that they orbit the Sun in a prograde direction.
- The analysis of the oldest rocks and meteorites date the Solar System at about 4.56 Gyr, while Earth's rocks are younger.
- Solar System is formed by smaller planets, mainly composed by rocky material, closer to the Sun, and giant, gaseous planets, which are more distant from the star.

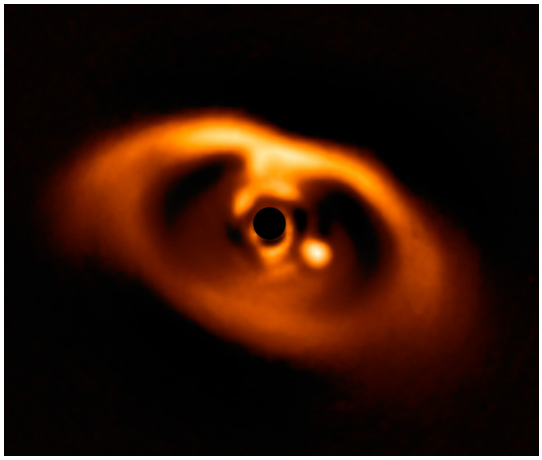

Figure 1.1: *This is the first clear image of a forming planet inside the gap of a circumstellar disk. The planet, PDS 70b, is orbiting the central star PDS 70, and it is visible in this image as a bright spot. The image has been obtained by the SPHERE instrument on ESO's Very Large Telescope (VLT).* **Credit:** ESO/A. Müller et al.

- The presence of satellite systems around most planets and how they formed.
- Provide a solution to the Angular Momentum Problem.

The main objective of this work of thesis is the study of dust distribution in a circumstellar disk with two planets with intermediate masses.

In this chapter we have presented a brief history about the origins of planetary formation models, from the early theories to our days.

Chapter 2 will be devoted to theoretical description of circumstellar disks, with emphasis both on gas and particle dynamics. Furthermore, we will account for disk dispersal processes and mechanisms that lead particles to grow, allowing the formation of larger bodies.

We will describe planet interaction with gaseous disks in Chapter 3 and how the mutual exchange of angular momentum between planets and gas leads to planetary migration in the disk and, for sufficiently massive planets, to gap opening in gas distribution.

In Chapter 4 we will start with a brief description of FARGO algorithm. Then, we will describe the initial parameters of our disk and we will analyze the results obtained.

Finally, in Chapter 5 we will draw conclusions basing on the results obtained and we will point out some possible future developments of this work.

Chapter 2

Theoretical aspects of protoplanetary disks

Current models about planet formation predict that planets formed in protoplanetary disks (also known as circumstellar disks) made of gas and dust. These disks surround the central star in the early stages of its life.

Stars form in giant molecular clouds. These clouds, made of cool gas with temperature of about 10 K, have complex internal structures with filamentary or clumpy shape [9].

If we consider smaller scales, we find denser regions, with typical values of about $10^5 - 10^7\,\mathrm{cm}^{-3}$, called cores, roundly shaped. A further collapse of these zones will form stars.

From an observational point of view, we can distinguish four classes where to place stellar objects in their early stages. The distinction among different classes is based upon the measurement of spectral energy distributions (SED), by defining a parameter [10]

$$\alpha_{IR} \equiv \frac{\Delta \log(\lambda F_\lambda)}{\Delta \log \lambda} \tag{2.1}$$

where λ is the wavelength and F_λ is the flux, which is generally a function of the wavelength.

At the beginning a dense, rotating core collapses and forms a central protostar with its surrounding disk, both still embedded in an optically thick envelope of gas and dust. At this stage, due to the protostar low mass and the surrounding gaseous envelope, SED presents a peak in the far-infrared region. These are classified as Class 0 objects.

The emergence of a circumstellar disk is an unavoidable consequence of conservation of angular momentum of the collapsing region. Indeed, typical values of the specific angular momentum of cores right before the collapse are about $10^{21}\,\mathrm{cm}^2\mathrm{s}^{-1}$. This value appears to be various orders of magnitude higher than the typical specific angular momentum of a star [11].

Let us assume to have an initial collapsing core of mass M_c, with specific angular momentum J_c. Supposing that the circumstellar disk is a keplerian one, then we have

$$\Omega^2(r_d) = \frac{J_c^2}{r_d^4} = \frac{GM_c}{r_d^3} \tag{2.2}$$

where $\Omega(r_d)$ is the keplerian angular velocity of the disk at radius r_d.

This results in values of the order of 10^2 AU for typical protoplanetary disks.

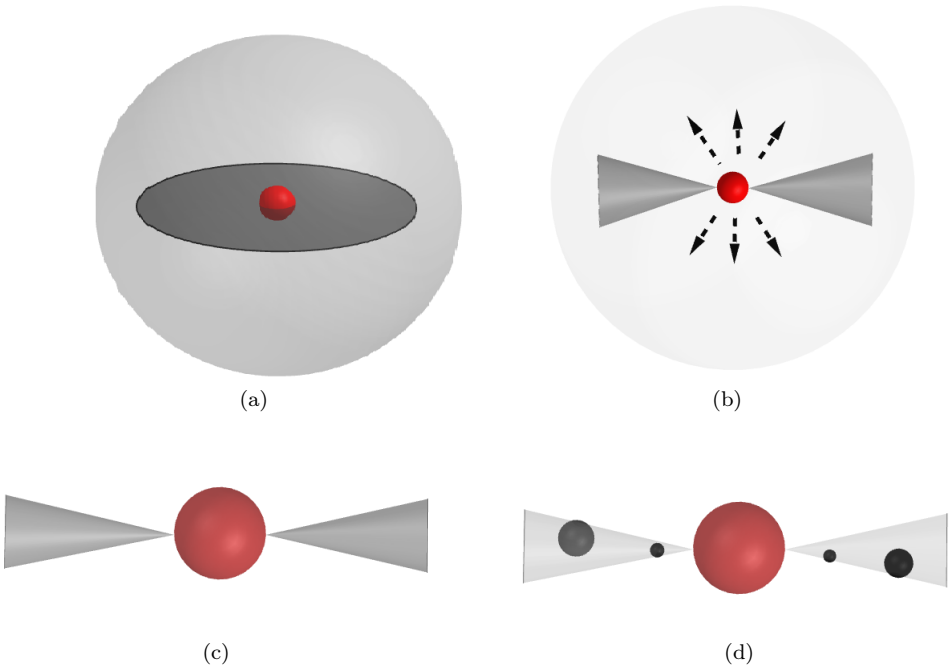

Figure 2.1: *Various phases of a protostar with its circumstellar disk. Class 0 objects (a) are just born protostars, surrounded by their circumstellar disk and by a thick envelope of gas and dust. In class I objects (b) we find protostars which emit intense stellar winds, surrounded by circumstellar disk. Class II objects (c) include protostars with a thick circumstellar disk, while the gaseous envelope has been dispersed. Planetesimal formation starts in this stage. Finally, class III objects (d), where the central protostar is surrounded by an almost dispersed circumstellar disk, relatively rich in dust.*

The existence of such disks has been proven both directly, thanks to images from the Hubble Space Telescope [12] and other surveys, and indirectly, by analyzing scattering of stellar light due to the dust component in the disk.

As time passes, the central star is continuously supplied with matter through the disk and it develops a stellar wind along the rotational axis. Stellar objects in this phase, with $\alpha_{IR} \geq -0.3$ are classified as Class I objects.

Class II consists of a protostar with an optically thick circumstellar disk, while the envelope has been dispersed due to the strong stellar wind. During this phase it is thought the formation of planets in the circumstellar disk takes place. Objects of this class have a value of $-1.6 \leq \alpha_{IR} \leq -0.3$.

Finally, the last stage for a young stellar object is a Class III object, with $\alpha_{IR} < -1.6$. Here, the star is in the region near to the main sequence in the Hertzsprung-Russell diagram and its circumstellar disk is dispersed through various mechanisms, such as photoevaporation, stellar winds and accretion onto protoplanets. In this phase we can find a relatively rich disk in dust, due to collisions between protoplanets.

All these phases are summarized in Fig. 2.1.

2.1 Protoplanetary disk structure

The improvement of telescopes and antennas that probe interstellar space could help us in achieving a better description of the early stages of a star and its circumstellar disk.

Actually, one of the most frequently used models in simulations to describe the profile of a protoplanetary disk is Weidenschilling's model for the Solar Nebula [13].

This model, which is called *Minimum Mass Solar Nebula* (MMSN), consists in an extrapolation of the density profile of a protoplanetary disk starting from observations and data of the actual chemical composition, mass of planets and their orbital radii. As its name tells, this method provides only a lower limit to the Solar Nebula mass.

Weidenschilling's model is composed by three steps:

- The masses of planets' heavy elements are increased through the addition of hydrogen and helium in order to restore the obtained mixture to Solar composition.
- Solar System is divided into annuli centered on planets' semimajor axes and extended up to the half distance with the neighbouring planets.
- The augmented mass of each planet is spread over the corresponding annulus.

This procedure determines a density profile $\Sigma(r)$ for the circumstellar disk which scales as

$$\Sigma(r) = \Sigma_0 \left(\frac{r}{1\,\mathrm{AU}}\right)^{-p} \tag{2.3}$$

where $p = 3/2$ in Weidenschilling's method.

Usually, one uses Hayashi's normalization [14]

$$\Sigma(r) = 1700 \left(\frac{r}{1\,\mathrm{AU}}\right)^{-3/2} \mathrm{g\,cm^{-2}} \tag{2.4}$$

which, integrated over a disk of radius 30 AU (Neptune distance to the Sun), gives a mass value of $0.01\,M_\odot$.

The exact description of the disk configuration would require the solution of a set of hydrodynamical partial differential equations. This can be done only for exceptional cases, while for the greatest part of the cases one resorts to numerical solutions with computer algorithms, assuming some reasonable semplifications.

In particular, in the case of protoplanetary disks, one can make two simplifying assumptions [15].

First of all, we can consider the disk mass negligible with respect to the star mass, namely $M_d \ll M_*$. This simplification will allow us to neglect disk gravitational potential with respect to stellar gravity.

Circumstellar disks are objects that are in a continuous evolution. So, there will be periods in the disk's life when our assumption turns out to be correct and periods when it will not apply.

Considering the previously described various stages of a protoplanetary disk and taking Hayashi's estimate on the minimum mass Solar Nebula, we can approximately establish when our assumption is accurate.

As we have seen, in the very early stages, the stellar mass is little with respect to its final value, while the disk mass is high. So, in this phase, we cannot apply our hypothesis. As

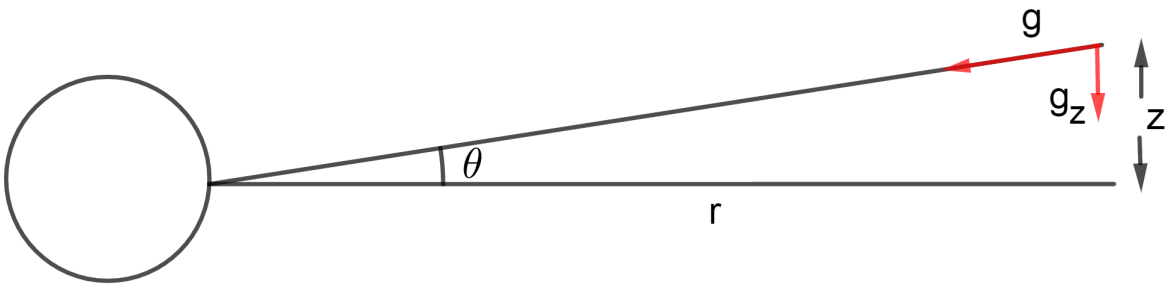

Figure 2.2: *Schematic profile of a protoplanetary thin disk.*

time passes, the disk loses part of its mass because both of stellar accretion and dispersion phenomena. We could apply our simplification when $M_d \leq 0.01 M_*$.

A second guess on protoplanetary disk is about its vertical thickness, which we will assume to be a little fraction of its radius.

Due to its geometrical structure and, in particular, to its large surface area, the disk can efficiently cool because of radiative losses. This causes low temperatures and pressures in the disk, so that it cannot support the gas against gravity. The resultant geometry is that of a thin disk where $h/r \ll 1$.

In order to obtain a density profile for the disk, we have to analyze the balance between gravitational forces and pressure forces. A schematic profile of the disk is represented in Fig.2.2.

Let us indicate the vertical axis as the z-axis. Considering a disk element at distance r from the star and at height z from the plane where the disk lays, the vertical component of the gravitational force per unit of mass is given by

$$g_z = -g \sin\theta = -\frac{GM_* z}{\left(r^2 + z^2\right)^{3/2}} \tag{2.5}$$

As a first approximation, we can now assume that the disk temperature is due to stellar irradiation and, as a consequence, we can suppose that the disk is vertically isothermal. This translates into an equation for the pressure that is $P = c_s^2 \rho$, where c_s is the sound speed.

So, the vertical component of the gravitational acceleration must balance the vertical pressure gradient $\frac{1}{\rho}\left(\frac{\mathrm{d}P}{\mathrm{d}z}\right)$, obtaining

$$c_s^2 \frac{\mathrm{d}\rho}{\mathrm{d}z} = -\frac{GM_* z}{\left(r^2 + z^2\right)^{3/2}} \rho \tag{2.6}$$

The solution of this differential equation provides us with the following density profile

$$\rho(z) = \rho_0 \exp\left[\frac{GM_*}{c_s^2 \left(r^2 + z^2\right)^{1/2}}\right] \tag{2.7}$$

with ρ_0 the mid-plane density.

Now, let us apply the hypothesis $z/r \ll 1$, so we have $g_z \approx \frac{GM_* z}{r^3} = \Omega^2 z$, where Ω is the angular velocity for a Keplerian disk, whose expression we will derive in the next section.

This leads us to a simplification for the expression 2.7 for the density profile

$$\rho = \rho_0 e^{-\frac{z^2}{2h^2}} \tag{2.8}$$

where we have defined the vertical scale height as

$$h \equiv \frac{c_s^2 r^3}{GM_*} = \frac{c_s^2}{\Omega^2} \tag{2.9}$$

Typical observed values of disk vertical thickness are in the range $h/r = 10^{-3} \div 10^{-1}$.

In order to verify if the disk self gravity is negligible, let us define the Toomre parameter, which is a generalization of Jeans criterion to differentially rotating disks [16]

$$Q \equiv \frac{c_{s,m}\kappa}{\pi G\Sigma} \tag{2.10}$$

where $c_{s,m}$ is the sound speed at the midplane and κ is the epicyclic frequency (in the case of a Keplerian disk $\kappa \approx \Omega$).

If $Q \leq 1$ disk self gravity is not negligible: the disk is unstable against its gravity and could fragment.

Using the definition 2.9 and approximating the disk mass as $M_d = \pi R_d^2 \Sigma$, we obtain

$$Q \simeq \frac{h}{R_d}\frac{M_*}{M_d} \tag{2.11}$$

so, for ordinary values of h/r, disk self gravity is negligible if $M_d \leq 0.01 M_\odot$.

The particular vertical structure of a disk is important also because it contributes to determininig the temperature profile, especially in the case of passive disks.

There are various processes that contribute to setting the temperature in a disk, among which:

- The central star irradiates its circumstellar disk and a certain fraction of this radiation, whose value depends both on the disk structure and on the density of gas and dust in it, is absorbed by the disk, especially by the dust component. This process leads to disk heating.

  Subsequently, dust reradiates at longer wavelengths, leading to disk cooling.

- The loss of potential energy because of the infall of matter onto the star contributes to disk heating. This contribution depends upon mass accretion rate of the central star.

- Disk's differential rotation leads to viscous interaction between adjacent fluid elements. Viscous dissipation is another important heating mechanism in a protoplanetary disk.

A disk where star irradiation is the main heating method is called a *passive disk*.

As we have said, vertical structure is important in these disks, since this factor leads to the absorption of a certain fraction of stellar radiation. As we expect, the more the surface is exposed to stellar radiation, the more it is heated.

There are two main profiles for passive disks: flat disks (or razor-thin disks) and flared disks.

In the case of flat disks, the disk is entirely in the star equatorial plane and the absorption of incident stellar radiation leads to a temperature profile $T_d \propto r^{-3/4}$.

Instead, in the case of flared disks, where the ratio h/r is a function of r, the increasing thickness of the disk causes the absorption of a greater fraction of stellar radiation, leading to a temperature profile $T_d \propto r^{-1/2}$ [15].

2.2 Disk dynamics and evolution

It is evident from observations that protoplanetary disks are not static structures, but they evolve. This evolution is responsible, among other things, for angular momentum transport due to dissipative effects, accretion of material onto the central star and, finally, disk dispersal, which we will discuss in the next section.

The basis for evolution of accretion disks theory have been posed by Lynden-Bell and Pringle in 1974 [17], even if a more qualitative understanding of physical processes of this structures had been reached by the astronomer Jeffreys in 1924.

Consider a test particle of mass m, at distance r from the central star. In absence of dissipative processes, the particle will only be subject to the gravitational potential of the star. The stability of this orbit is guaranteed if the particle experiences a centrifugal force that counterbalances the gravitational one, that is

$$m\frac{v_\phi^2}{r} = \frac{GM_* m}{r^2} \tag{2.12}$$

and this leads to the expression of the Keplerian velocity

$$v_K = \sqrt{\frac{GM_*}{r}} \tag{2.13}$$

Since the disk gas rotates differentially and since every real fluid has viscosity, the shear between two adjacent annuli leads to exchange of angular momentum.

Consider a disk with surface density $\Sigma(r,t)$ and take an annulus at radius r, that extends to $r+\Delta r$. Matter can flow into or out of it with radial velocity $v_r(r,t)$.

We can write the continuity equation for the annulus mass, considering gas that flows inside or outside

$$\frac{\partial}{\partial t}(2\pi r\Delta r\Sigma(r,t)) = 2\pi r\Sigma(r,t)v_r(r,t) - 2\pi(r+\Delta r)\Sigma(r+\Delta r,t)v_r(r+\Delta r,t) \tag{2.14}$$

Considering small values of Δr we have

$$\Sigma(r+\Delta r,t) \simeq \Sigma(r,t) + \frac{\partial\Sigma}{\partial r}\Delta r$$

and, substituting this into 2.14, continuity equation simplifies as

$$r\frac{\partial\Sigma}{\partial t} + \frac{\partial}{\partial r}(r\Sigma v_r) = 0 \tag{2.15}$$

An analogous reasoning can be done for angular momentum conservation, which allows us to write

$$r\frac{\partial}{\partial t}\left(\Sigma r^2\Omega\right) + \frac{\partial}{\partial r}\left(r\Sigma v_r r^2\Omega\right) = \frac{1}{2\pi}\frac{\partial G}{\partial r} \tag{2.16}$$

where $\Omega(r,t)$ is the angular velocity of the gas at radius r and $G(r,t)$ is the torque exerted by the adjacent outer annulus on the inner one.

Writing the viscous force per unit length as $\nu\Sigma r\frac{\mathrm{d}\Omega}{\mathrm{d}r}$, the torque is

$$G = 2\pi r\cdot\nu\Sigma r\frac{\mathrm{d}\Omega}{\mathrm{d}r}\cdot r \tag{2.17}$$

Finally, assuming a Keplerian angular velocity $\Omega \propto r^{-3/2}$ we come to

$$\frac{\partial \Sigma}{\partial t} = \frac{3}{r}\frac{\partial}{\partial r}\left[r^{1/2}\frac{\partial}{\partial r}\left(\nu \Sigma r^{1/2}\right)\right] \tag{2.18}$$

and thus we conclude that this is a diffusive equation for surface density. In the case that ν is constant, this is more evident if we perform a variable change

$$X \equiv 2r^{1/2} \tag{2.19}$$

$$f \equiv \frac{3}{2}\Sigma X \tag{2.20}$$

This leads us to

$$\frac{\partial f}{\partial t} = D\frac{\partial^2 f}{\partial X^2} \tag{2.21}$$

where the diffusion coefficient is defined in the following way

$$D = \frac{12\nu}{X^2} \tag{2.22}$$

This allows us to define a diffusive timescale

$$t_{diff} = \frac{(\Delta X)^2}{D} \tag{2.23}$$

Coming back to physical variables and assuming r to be the characteristic size of the disk, we have the viscous timescale

$$\tau_\nu \sim \frac{r^2}{\nu} \tag{2.24}$$

This time represents the time needed for smoothing out surface density gradients through viscosity.

When we consider a real fluid, we associate to it a molecular (or kinematic) viscosity

$$\nu_m \sim \lambda c_s \tag{2.25}$$

where c_s is the sound speed in the medium and λ is the mean free path between gas molecules

$$\lambda \simeq \frac{1}{n\sigma_g} = \frac{\mu m_H}{\rho_g \sigma_g} \tag{2.26}$$

where μ is the gas molecular weight, ρ_g is the gas density and σ_g is the cross section of gas molecules that, in the ideal case, coincides with the area occupied by a molecule $\sigma_g = 4\pi r_g^2$.

Inserting typical values for protoplanetary disk parameters we obtain $\nu_m \sim 10^7\,\mathrm{cm^2 s^{-1}}$, corresponding to a viscous timescale $t_\nu \sim 10^{13}\,\mathrm{yrs}$.

This extremely large time constitutes a problem, since observed disk lifetimes are about $10^6 \div 10^7\,\mathrm{yrs}$.

So, we can conclude that molecular viscosity is not the source of angular momentum transport in protoplanetary disks.

A fundamental parameter in fluid dynamics is Reynolds number, defined as

$$Re = \frac{UL}{\nu_m} \tag{2.27}$$

where U is the characteristic velocity of the fluid and L is the length scale.

This parameter describes if a fluid is in laminar regime (small Re) or in turbulent regime (high Re).

The presence of such a small molecular viscosity implies a high Reynolds number, which means that gas in protoplanetary disk is in a turbulent regime, with the formation of eddies and vortices.

Now, the microphysics of turbulent fluids happens to be very complex to be treated in detail. So, in order to give an approximate analytic description of turbulent viscosity, we will adopt α-prescription [18] and we write

$$\nu \sim \alpha c_s h \tag{2.28}$$

where α is a dimensionless parameter and h is the height of the disk.

Let us briefly justify this expression for viscosity.

We can assume turbulence to be isotropic, so the length scale of the turbulent flow is limited by the smallest length scale of the disk, that is the height h. Further more, we can limit the speed of the flow to be less than c_s, since eventual supersonic flows lead to rapid dissipation.

Finally, because of these reasons, there is a limit on the parameter α of eq. 2.28, that is $\alpha < 1$.

Although α-prescription allows us to have a simple expression for turbulent viscosity, it does not provide a faithful description of protoplanetary disks [19]. Indeed, one of the main mechanisms for angular momentum transport is provided by magnetohydrodynamic processes, whose efficiency varies with the degree of ionization, which happens to be a function of temperature and surface density.

We are now interested in studying the azimuthal velocity of gas in the disk, since it will be useful later on when we will treat about dust dynamics in the disk.

The equation that describes the evolution of momentum for an inviscid, unmagnetized fluid is

$$\frac{\partial \mathbf{v}}{\partial t} + (\mathbf{v} \cdot \nabla)\mathbf{v} = -\frac{1}{\rho}\nabla P - \nabla \Phi \tag{2.29}$$

where $\mathbf{v}$ is the velocity of the fluid, P is the pressure, ρ is the density and Φ is the gravitational potential.

Considering the case of a simplified protoplanetary disk, let us assume stationary and axisymmetric flow. So, the previous equation simplifies to

$$\frac{v_\phi^2}{r} = \frac{GM_*}{r^2} + \frac{1}{\rho}\frac{\mathrm{d}P}{\mathrm{d}r} \tag{2.30}$$

Since we expect that pressure decreases with increasing radius, we can write the pressure profile as

$$P = P_0 \left(\frac{r}{r_0}\right)^{-n} \tag{2.31}$$

where $P_0 = \rho_0 c_s^2$ and n is a power index.

Substituting this pressure profile into eq. 2.30 we find

$$v_\phi = v_K \left(1 - n\frac{c_s^2}{v_K^2}\right)^{1/2} = v_K(1-\eta)^{1/2} \tag{2.32}$$

where $\eta = n\frac{c_s^2}{v_K^2}$. So, we see that gas azimuthal velocity is less than keplerian velocity because of the presence of gas pressure gradients that partially counterbalance the central star's gravitational force.

2.3 Disk dispersal

A fundamental issue in protoplanetary disk theory concerns disk's lifetime and the mechanisms through which the disk is dispersed.

The gaseous component of a disk is an essential element in the formation of protoplanets. Indeed, if gas had dispersed before dust coagulation happens, no protoplanets could have been formed.

Furthermore, even if dust could coagulate, allowing the formation of terrestrial planets and giant planets' rocky cores, a short disk lifetime could not allow the formation of giant planets, since gas would not have time to accrete onto giant planets' cores.

Observations of stellar systems and clusters provide a superior limit to protoplanetary disks lifetime.

Indeed, the disk frequency is about 100% in stellar clusters with a mean age of stars of 1 Myr, while this value drops to 50% in clusters where stars have a mean age of 3 Myr. Ultimately, protoplanetary disks are almost completely absent around stars with an age greater than 10 Myr [15].

All these insights provide us with a typical disk lifetime of about $3 - 5$ Myr.

There are various processes that are responsible for disk dispersal. One of them, which we have already seen in the preceding section and which is one of the main dispersal mechanisms, is accretion of material onto the central star.

Other important contributions to disk dispersal, which we will briefly examine in this section, derive from close stellar encounters, stellar winds and photoevaporation by ultraviolet (UV) radiation from the central source [20]. We can also add to these effects accretion of material onto planetesimals, even if this process provides negligible effects compared to the others.

Since most stars do not form in isolated environments, but rather they form in clusters, stellar encounters and their consequent interaction with another star's circumstellar disk lead to disk dispersal.

The interaction of a perturber star with the disk leads to the unbounding of the external disk material. Indicating the impact parameter between the two stars with r_p, the typical final size of a disk subject to this dispersal mechanism is about $r_d = \frac{1}{3}r_p$ [21].

So, we can estimate the characteristic time for disk dispersal due to close stellar encounters in clusters. This will be the inverse of the encounters rate, that is $t_{SE} = \frac{1}{n_* \sigma v}$, where n_* is the stellar density in the cluster, σ is the cross section for the encounter, $\sigma = \pi(3r_d)^2$, and v is the relative velocity between two stars. Characteristic values of these parameters lead to a timescale [20]

$$t_{SE} = 2 \cdot 10^7 \left(\frac{n_*}{10^4\,\mathrm{pc}^{-3}}\right)^{-1} \left(\frac{v}{1\,\mathrm{km\ s}^{-1}}\right)^{-1} \left(\frac{r_d}{100\,\mathrm{AU}}\right)^{-2} \mathrm{yrs} \tag{2.33}$$

N-body simulations of dense stellar clusters [22] show that close stellar encounters are very rare. In their simulations, Scally & Clarke found that the greatest part of these encounters takes place at about 1000 AU, while only 4% occurs at distances under 100 AU.

So, we can conclude that, even if this mechanism is potentially intense, it is not one of the main causes for disk dispersal due to its rarity.

The interaction between the central star magnetic field and the ionized particles in the inner edge of its circumstellar disk gives rise to a wind of material ejected from the disk, with a mass loss rate $\dot{M}_w = 10^{-8} \div 10^{-7}\,\mathrm{M_\odot yr^{-1}}$.

Once the star has accreted sufficient material, magnetic activity in the chromosphere drives a stellar wind, similar to that of the current Sun, even if more intense. This wind disperses the disk in a characteristic timescale $t_{ws} \simeq 10^7$ yrs for typical disk and wind parameters, with a mass loss rate of $\dot{M}_{ws} = 4 \cdot 10^{-9}\, M_\odot \mathrm{yr}^{-1}$ [20].

One of the most efficient disk dispersal processes is photoevaporation. Through this mechanism, UV radiation heats disk surface, causing a flow of gas and small dust particles.

Disk evolution is influenced by two kinds of radiation: extreme ultraviolet (EUV) radiation, with photons of energy $E > 13.6\,\mathrm{eV}$ which ionize hydrogen atoms, and far ultraviolet (FUV) radiation, with photons of energy $6 < E < 13.6\,\mathrm{eV}$, which dissociate molecules as H_2 and CO and ionize carbon C.

While EUV radiation ionizes disk surface, heating it to a temperature of the order of $10^4\,\mathrm{K}$, FUV photons penetrate the ionized hydrogen layer and heats a neutral layer of hydrogen (both atomic and molecular) to temperatures in the range $100\,\mathrm{K} < T < 5000\,\mathrm{K}$. In the region heated by FUV radiation, called Photodissociation Region (PDR), gas is continuously heated and cooled by radiative emission.

Equating gravitational potential energy and thermal energy it is possible to define the quantity [23]

$$r_g = \frac{GM_*}{k_B T} \sim 100 \left(\frac{T}{1000\,\mathrm{K}}\right)^{-1} \left(\frac{M_*}{M_\odot}\right) \mathrm{AU} \tag{2.34}$$

This quantity is called gravitational radius and it defines the region of the disk where gas at temperature T can escape from the gravitationally bound system.

Early models assumed that photoevaporation effects were present only for $r > r_g$, while more recent calculations show that a significant mass loss due to photoevaporation is also present at $r \sim 0.1 \div 0.2\, r_g$.

Another important quantity is the size of the disk r_d, especially in the case of radiation coming from an external source (i.e. a neighbour star). Indeed, while radiation from the central star especially warms up inner regions of the disk, in this case there is a substantial mass loss even from the external side of the disk.

In the case of high mass stars, the central star has a very high production rate of EUV photons, which lead the disk to a mass loss rate [24]

$$\dot{M}_{EUV} = 4 \cdot 10^{-10} \left(\frac{\Phi_{EUV}}{10^{41}\,\mathrm{s^{-1}}}\right)^{1/2} \left(\frac{M_*}{M_\odot}\right)^{1/2} M_\odot \mathrm{yr}^{-1} \tag{2.35}$$

Both because of the high mass and EUV photons production rate, the disk mass loss rate can reach values as high as $\dot{M}_{EUV} \sim 10^{-5}\, M_\odot \mathrm{yr}^{-1}$, with characteristic times for the evaporation of disk outer layers of 10^5 yrs.

In absence of an intense chromospheric activity that produces high rates of EUV photons, mass loss is meanly due to FUV radiation, with rates of the order of $\dot{M}_{FUV} \sim 10^{-7}\, M_\odot \mathrm{yr}^{-1}$ [23].

2.4 Dust dynamics and evolution

In a circumestellar disk, if gas provides the material for the accretion of the central star, micron sized dust is the starting point for the formation of terrestrial planets and for the cores of giant planets (to be exact, gas provides also the gaseous envelopes of giant planets).

Starting from this observation, we understand the importance of the detailed study of dust component in a protoplanetary disk. In order to comprehend planet formation, we need a thorough analysis of dust grains coagulation mechanisms and of the motion of dust coupled with the gaseous component in a disk. We will review these aspects in this section.

As opposed to gas, dust is not supported by the pressure gradient against the gravitational collapse. If the gas were not present in the disk, dust particles would follow keplerian orbits around the central star.

The interaction between gas and dust particles is responsible for the drag force on dust.

Let us consider a spherical particle of dust, with radius s and density ρ_d, immersed in the gaseous component of a protoplanetary disk, in which it moves with a velocity v relative to the gas velocity, i.e. $v = |\mathbf{v}_d - \mathbf{v}_g|$, where $\mathbf{v}_d$ and $\mathbf{v}_g$ are respectively the dust velocity and gas velocity calculated in a rest frame.

In order to calculate the drag force acting on dust particles, we have to consider two different regimes, based on the ratio between the dust particle radius s and the gas molecules mean free path λ.

If the particle is smaller than the mean free path (i.e. $s \leq \lambda$), then the interaction between gas and dust will be described through a molecular point of view.

In this regime, called Epstein regime, we have a dust particle of radius s moving in a gas at temperature T with velocity v. Gas is considered as an ensemble of molecules, with mean molecular velocity

$$v_{th} = \sqrt{\frac{8k_B T}{\pi \mu m_H}} \tag{2.36}$$

In this regime drag force results from molecular collisions with dust. The frequency of collisions with the front side of the particle is given by

$$f_+ = n\sigma v_{rel} \approx \frac{\rho}{\mu m_H} \pi s^2 (v_{th} + v) \tag{2.37}$$

A similar expression holds for collisions with the back side of the particle

$$f_- = n\sigma v_{rel} \approx \frac{\rho}{\mu m_H} \pi s^2 (v_{th} - v) \tag{2.38}$$

Since in a single collision the transferred momentum is $2\mu m_H v_{th}$, the drag force for particles with $v \ll v_{th}$ and a Maxwellian distribution for molecular speeds is

$$\mathbf{F}_D = -\frac{4\pi}{3} \rho s^2 v_{th} \mathbf{v} \tag{2.39}$$

In cases where dust particles are larger than gas molecules' mean free path (i.e. $s \geq \lambda$), the interaction will be described in fluid terms. In this regime, called Stokes regime, the spherical particle moves in a fluid and the drag force is given by

$$\mathbf{F}_D = -\frac{C_D}{2} \pi s^2 \rho v \mathbf{v} \tag{2.40}$$

where C_D is the drag coefficient which, in general, depends upon the shape of the particle. In the case of a spherical particle, C_D depends only upon Reynolds number

$$Re = \frac{2s\rho v}{\nu} \tag{2.41}$$

where ν is the molecular viscosity of gas

$$\nu \simeq \frac{1}{3}\rho\lambda v_{th} \tag{2.42}$$

Specifically, the drag coefficient has the following values

$$C_D \simeq \begin{cases} 24\mathrm{Re}^{-1}, & \text{if Re}< 1 \\ 24\mathrm{Re}^{-0.6}, & \text{if } 1 < Re < 800 \\ 0.44, & \text{if Re}> 800 \end{cases} \tag{2.43}$$

Equating the expressions for the drag force in the two different regimes we obtain the requirement $\frac{\lambda}{s} = \frac{4}{9}$, which provides the condition for the transition between the two regimes.

Dust is initially spread all over the disk, but the effect of star's gravitational force is responsible for dust settling at the midplane. However, there are various processes that oppose to dust settling or reinforce it.

In this section we will only mention these mechanisms, without analyzing them in detail.

To a first approximation, we will ignore turbulence effects, not because they have negligible effects on dust dynamics, but because they overcomplicate the treatment.

We can define a quantity that well describes the coupling between dust and gas in a disk, which is the friction time scale

$$t_{fric} = \frac{mv}{|F_D|} \tag{2.44}$$

where $m = \frac{4\pi}{3}\rho_d s^3$ is the mass of the dust particle, v is the relative velocity between dust and gas and F_D is the drag force acting on dust.

This quantity provides an estimate of the time needed by the drag force to modify the particle velocity in a relevant manner.

In the first stages of a circumstellar disk we typically find micrometer sized (or smaller) dust grains, characteristic of interstellar medium (ISM). So, we can assume to be in Epstein regime and we can write the previous expression as

$$t_{fric} = \frac{\rho_d}{\rho}\frac{s}{v_{th}} \tag{2.45}$$

Inserting typical values in this expression, we obtain friction times $t_{fric} \sim 1\,\mathrm{s}$. This means that there is a strong coupling between gas and dust in this stage.

Now, let us consider a dust particle at height z above the disk midplane. This particle will experience a gravitational force, which will be responsible for its settling at the midplane, whose z-component is

$$|F_{grav}| = m\Omega^2 z \tag{2.46}$$

where Ω is the keplerian velocity.

Since dust does not experience the pressure force due to the gas component, friction force will be the only force opposed to gravitational force.

So, if we suppose that the particle started at rest at height z above the midplane, it will accelerate downward until friction force will equate gravitational force. As we have seen, small dust particles are very tightly coupled with gas. So, we can assume that the equality between the two forces will happen in very short times, leading to the following settling velocity

$$v_{settle} = \frac{\rho_d}{\rho} \frac{s}{v_{th}} \Omega^2 z \tag{2.47}$$

Given this expression, we will have a settling time for micrometer sized particles

$$t_{settle} = \frac{z}{|v_{settle}|} \tag{2.48}$$

and, numerically, it will be $t_{settle} \sim 10^5$ yrs for characteristic disk parameters.

It is remarkable to see that this settling time estimate is consistent with disks lifetime, allowing dust to settle at the midplane before disk dispersal.

However, the above expressions have been derived without taking into account two important processes: dust coagulation and turbulence of the gas component.

Even if we will not get into details of these processes, we will give an hint on how these mechanisms affect dust settling.

Turbulence has a fundamental role in protoplanetary disks: not only it is responsible for angular momentum transport, but it also opposes to dust settling. Indeed, turbulent motions of gas in the disk cause the lifting of dust particles, slowing down the settling at the midplane.

On the other hand, while settling, dust particles collide with others, growing its size and mass. This leads to bigger particles that are less coupled with gas. The combination of both the accretion of particles with a lower coupling between dust and gas leads to a faster settling at the midplane.

As we have previously seen, if a particle is orbiting around a central star and it is only subject to the star's gravitational potential, the particle will move with Keplerian velocity.

Now, if we put the particle in the gaseous disk, its dynamics will be influenced by the interaction with the disk and, in general, it will not have Keplerian velocity.

As we have seen, the strength of coupling between gas and dust depends on dust size. So, we can distinguish two main cases:

- **Small dust grains**: here dust particles and gas are very tightly coupled, so dust grains are dragged by gas, which moves at sub-Keplerian velocities. As opposed to gas, dust is not supported by pressure against gravitational collapse, so sub-Keplerian motion leads to an inward spiralling.
- **Large dust grains**: here dust particles are poorly coupled with gas. But, even in this case, the result is an inward spiralling of dust particles. Indeed, now dust grains move at Keplerian speeds, but they experience an headwind due to sub-Keplerian motion of gas that remove angular momentum from the particles, causing the inward drift of dust.

Solving the equations of motion in polar coordinates [15] and defining a dimensionless friction time (also known as Stokes number)

$$\tau_{fric} = St \equiv t_{fric} \Omega_K \tag{2.49}$$

where Ω_K is the Keplerian angular velocity, we obtain an expression for the radial velocity

$$v_r = \frac{\tau_{fric}^{-1} v_{r,g} - \eta v_K}{\tau_{fric} + \tau_{fric}^{-1}} \tag{2.50}$$

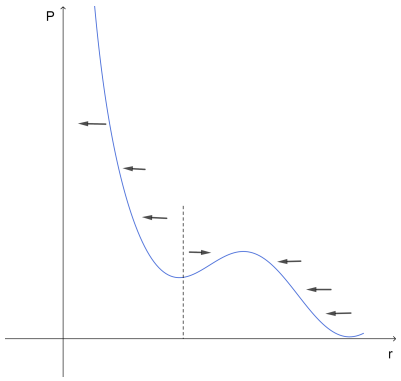

Figure 2.3: *Non monotonic pressure profile of a protoplanetary disk. Arrows represent radial drift of dust particles. Near the local maxima there is an accumulation of dust.*

where $v_{r,g}$ is the radial velocity of gas, while η has been defined in 2.32.

In the case of small dust particles (i.e. $\tau_{fric} \ll 1$) the previous expression simplifies to

$$v_r \simeq v_{r,g} - \tau_{fric}\eta v_K \tag{2.51}$$

So, we can observe that small particles are radially dragged with gas, but they also experience a radial drift relative to the gas, linearly depending on the coupling between gas and dust: the more the particle is decoupled by gas (i.e. increasing τ_{fric}), the more the relative drift between particle and gas is strong.

On the other hand, for larger particles (i.e. $\tau_{fric} \gg 1$) the expression 2.50 becomes

$$v_r \simeq -\tau_{fric}^{-1}\eta v_K \tag{2.52}$$

In this case, the more the particle is decoupled by gas, the less is the particle radial velocity (the particle will tend to stay in its Keplerian orbit).

It is possible to define drift time as

$$t_{drift} = \frac{r}{|v_r|} \tag{2.53}$$

and, using characteristic disk parameters, one finds that $t_{drift} \sim 10^3$ yrs.

This value is very little compared to disk lifetime, so planetesimal formation is possible only if the growth from micrometer sized to meter sized particles is sufficiently rapid. If it were not, small particles would drift towards the inner regions of the disk in short times and there star heating would cause them to evaporate.

So far, we have assumed a smooth pressure profile, with $P \propto r^{-n}$. However, the presence of turbolent phenomena or the presence of planets (especially giant planets) orbiting the star, can perturb the disk creating local maxima in the pressure profile (Fig. 2.3).

These perturbations of pressure profile appear to be very remarkable in the context of planet formation and Guilera & Sandor proposed these as the birthplaces for giant planet formation [25].

So, let us examine what happens in these regions of the disk.

Consider a pressure profile with a local maxima at radius r_{max}.

Let us conider the immediately outside regions to this maxima. Here pressure is decreasing, so $\frac{\mathrm{d}P}{\mathrm{d}r} < 0$. As we see from eq. 2.32, azimuthal velocity of gas in this region will be lower than the Keplerian velocity $v_{\phi,g} < v_K$.

So, dust particles in this area will experience a radial force towards the local maxima.

Similarly, if we consider now the immediately inside regions to the local maxima, here pressure is increasing, so $\frac{\mathrm{d}P}{\mathrm{d}r} > 0$. Again, taking into account eq. 2.32, azimuthal velocity of gas in this zone is greater than Keplerian velocity $v_{\phi,g} > v_K$.

Again, dust particles experience a radial force towards the local maxima.

So, in the pressure local maxima region, we have a concentration of material coming both from the internal and external zones.

2.4.1 Dust coagulation processes

As we have seen, coagulation process speeds up dust settling at the midplane and slows down radial drift, since it is responsible for the transition from micrometer sized to meter sized dust particles.

So, we can see coagulation as the initial process towards planets formation.

In this section we will review some details about this mechanism.

When two particles collide, it is not obvious that they will stick together to form a larger one. Indeed, the result of the collision can be the adhesion between the particles, but there are different possible outcomes, such as rebound and partial or total breakdown of the two colliding objects [26].

The result of a collision depends on a plethora of parameters such as kinetic energy, shape and material of the particles and impact parameter.

In order to understand how particles are sticked together, we have to look at the micro-physics of impacts, comprehending which forces are responsible for coagulation processes.

We can assume neutral dust grains, at least in the first stages of protoplanetary disk. In this case, dipole-dipole interactions are responsible for adhesion between particles.

Several experiments have been conducted [27] on colliding micrometer and sub-micrometer sized particles. These led to the following conclusions:

- Irregular grains have higher sticking probabilities compared to almost spherical shaped grains.
- The velocity threshold to have adhesion between spherical particles is less than 1 m/s, while for irregular grains this threshold extends to about 100 m/s.

Motion of particles of these sizes is well described by Brownian motion theory, where dust particles frequently collide with gas molecules, deviating from their original trajectory. On a macroscopic scale, an observer will note a random motion, due to these multiple scatterings.

The mean velocity of particles subject to Brownian motion in a gas at temperature T is

$$v = \sqrt{\frac{8k_B T}{\pi m}} \tag{2.54}$$

where k_B is Boltzmann constant and $m = \frac{m_1 m_2}{m_1 + m_2}$ is the reduced mass of the two colliding dust particles.

Assuming a disk with gas at temperature $T = 100K$ (characteristic temperature of disk external regions), we obtain a mean velocity for micrometer sized particles of the order of $v \sim 1\,\mathrm{mm/s}$.

When dust grains collisions lead to adhesion, dust aggregates start to form.

Similar experiments [28] to Poppe's have been conducted with the aim of studying aggregates collisions instead of particle-particle collisions. As opposed to dust particles collisions, where the possible outcomes were only sticking or bouncing, here we can also have adhesion with compactification of the aggregate or disgregation of it.

In particular, these experiments have shown that for impact velocities above 2 m/s, collisions lead to disgregation of the aggregate.

Chapter 3

Planetary dynamics in circumstellar disks

3.1 Tools for studying planetary dynamics

The first models that tried to describe planet motion in the sky date back to Babylonian civilisation and, then, to ancient Greeks.

All these theories had in common the belief in an ordered motion, based on numbers and specific ratios between planets' positions.

But we have to wait until the XVII century to have a systematic description of planetary motion, based on accurate observations by Johannes Kepler, who synthesized them in three laws:

- *All planets move along elliptical orbits and the Sun is at one focus of the ellipse.*

  In Euclidean geometry it is possible to describe an ellipse through its semimajor axis a and its semiminor axis b, or through its semimajor axis and its eccentricity, defined as

  $$e \equiv \left(1 - \frac{b^2}{a^2}\right)^{1/2} \tag{3.1}$$

  with $0 \leq e \leq 1$. This quantity suggests how much the ellipse is squashed.

  When the planet is at its farthest position from the Sun, it is said to be at aphelion, while when it is at its closest position to the Sun it is said to be at perihelion.

- *A radius vector from the Sun to a planet sweeps out equal areas in equal times.*

- *The square of the orbital period of a planet is proportional to the cube of its semimajor axis, that is*

  $$T^2 \propto a^3 \tag{3.2}$$

These empirical laws were subsequently theoretically justified by Newton, who derived them by applying his gravitational law to the system planet-Sun.

Since an orbiting body has six degrees of freedom (three spatial coordinates and three velocity coordinates) at a fixed time, we will need a set of six elements to fully determine the planet's orbit.

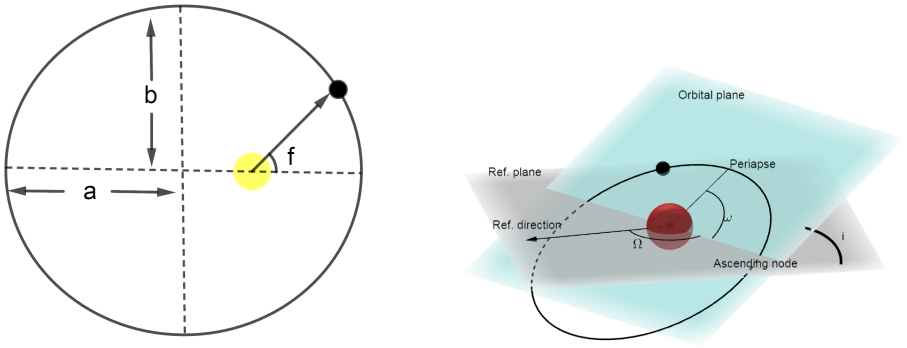

(a) (b)

Figure 3.1: *Orbital elements for the orbit of a planet around a star. The image on the left is the projection of the three dimensional orbit on the reference plane.*

The traditional set of orbital elements is constituted by Keplerian (or principal) orbital elements, some of which we have already described (semimajor axis and eccentricity).

Since we are considering motion in three dimensions, we have to choose a reference plane. A typical choice in Solar System is Earth's orbital plane around the Sun, called ecliptic.

Instead, more generic choices for the reference plane are the equatorial plane of the largest body in the planetary system or the plane perpendicular to the angular momentum vector of the system.

So, it is natural to introduce the inclination i of the orbital plane with respect to the reference plane. Its value range from 0° to 180°.

The intersection of these two planes gives rise to a line, called line of nodes. The extremities of this line are the ascending node, that is the point where the planet's orbit passes upward the reference plane, and the descending node, that is the point where the orbit passes downward.

Once we have chosen a reference direction in the reference plane, we can define the longitude of the ascending node Ω as the angle between this reference direction and the direction of the orbit's ascending node.

We then define the argument of periapse ω, that is the angle between the line to the ascending node and the line to the direction of periapse.

Finally, we need one last orbital element. This is the true anomaly f, which identifies the angle between the periapse and the instantaneous position of the orbiting body.

The knowledge of these elements at a given instant allows us to know the distance of a planet from the star

$$r = \frac{a(1-e^2)}{1+e\cos f} \tag{3.3}$$

3.2 Planetary migration in protoplanetary disks

As we have said in the first chapter, the discovery of exoplanetary systems has allowed us to test our planet formation theories, answering some questions. But new issues derived from these observations too.

One of these concerns the existence of hot Jupiters, that are planets with masses about Jupiter mass or greater, orbiting their central star with a period $T \leq 10$ days. An example

is the already cited exoplanet 51 Pegasi b, which has a mass about one half of Jupiter mass and orbits its star with a period of about 4 days, being located at 0.05 AU from the star.

This kind of planets constitutes a puzzling issue. Indeed, they cannot have formed in their actual position, that is too close to the star, because of the lack of materials to build them.

Another interesting feature is the existence of mean motion resonances in planetary systems. It seems very unlikely that two planets form in the exact resonance configuration, so there must exist a mechanism that takes two planets to these setups, starting from generic positions.

In order to answer to all these questions, physicists proposed an orbital migration mechanism during the early stages of planets lives.

With this expression, we mean an angular momentum exchange mechanism between a planet and the protoplanetary disk that leads to a change in semimajor axis.

Before going into mathematical details of planetary migration, we will give a qualitative argument about planet-disk interaction.

Let us consider a planet embedded in a protoplanetary gaseous disk and let us analyze the interaction of planet with surrounding gas layers.

If we consider a gas layer exterior to planet's orbit, this orbits around the star slower than the planet. The interaction between the planet and this external gas layer leads to exchange of angular momentum, with planet that partially loses it and external gas that gains it.

Consequently, the planet will have to migrate to an inner orbit, while gas will migrate to a more external one, creating some sort of repulsion between them.

Instead, if we consider the interaction between the planet and an interior gas layer, this will lead to an opposite migration.

Indeed, the internal gas layer will orbit around the star faster than the planet. So, the interaction will lead to a partial loss of angular momentum for the gas, while the planet will acquire it.

The consequence of this angular momentum exchange will be an inward migration of the gas layer, opposed to an outward migration of the planet.

Now that we have laid the foundations, we can go deep into mathematical treatment.

The presence of a planet in the gaseous disk creates a perturbation on the gas density and pressure profiles. These perturbations are described through the introduction of a tidal potential.

We can decompose this potential in Fourier modes

$$\phi(r, \varphi, t) = \sum_{m=0}^{\infty} \phi_m(r) \exp[im(\varphi - \Omega_p t)] \tag{3.4}$$

where m is the azimuthal wavenumber, $\phi_m(r)$ are the Fourier coefficients and Ω_p is the planet's angular velocity.

The external forcing potential ϕ is rotating in the gaseous disk, which is orbiting the star with angular velocity $\Omega(r)$.

This perturbation induced by planet's orbit excites waves in discrete resonant locations within the disk. So, we have to find where these resonances are located in the disk.

Let us remind that a resonance occurs whenever a characteristic frequency of the planet potential matches a frequency in the disk, that is

$$\omega = m(\Omega(r) - \Omega_p) = 0 \tag{3.5}$$

$$\omega = m(\Omega(r) - \Omega_p) = \pm\kappa(r) \tag{3.6}$$

where $\kappa(r)$ are epicyclic oscillation frequencies, that are the natural radial oscillations of a particle orbiting in the disk.

The first case is the co-rotation resonance, simply satisfied by $\Omega(r) = \Omega_p$.

Suppose we have a Keplerian disk, with $\Omega(r) = \sqrt{\frac{GM_*}{r^3}}$, and a planet orbiting the star on a circular orbit of radius a. So, we see that we have co-rotation resonance for gas elements that are co-orbital with the planet.

The second case, known as Lindblad resonance, happens for a Keplerian disk at locations where

$$m\left[\sqrt{\frac{GM_*}{r^3}} - \sqrt{\frac{GM_*}{a^3}}\right] = \pm\sqrt{\frac{GM_*}{r^3}} \tag{3.7}$$

since for a Keplerian disk epicyclic and orbital frequencies coincide.

So, we can derive the expression for Lindblad resonance locations

$$r_L = \left(1 \pm \frac{1}{m}\right)^{2/3} a \tag{3.8}$$

So, we see that for increasing values of m, we have a set of resonant locations closer to the planet, whose spacing decreases.

From a physical point of view, there are fluid elements that are flowing on circular orbits, past the planet. Fluid elements located at Lindblad resonances are subject to large radial oscillations, exciting in this way acoustic waves that propagate all over the disk at approximately the sound speed. But, because of the contemporary Keplerian shear, the result is a spiral density wave.

Now, let us consider, as an example, waves propagating in outer disk regions. These waves carry angular momentum into the disk, which is stored in disk zones where density waves damp. Since in this case we have $\Omega_p > \Omega(r)$, then the planet will exert a positive torque on the disk.

The opposite is true for inner disk regions, where the planet exerts a negative torque on the disk [29].

Based on mass planet we can distinguish two different kinds of migration:

- **Type 1**: this kind of migration is characteristic of low mass planets (i.e. planets with a mass up to few Earth masses), which don't significantly perturb disk structure because of the weakness of their interaction. The planet is fully embedded in the gaseous disk at all times.

- **Type 2**: in this case, valid for high mass planets (i.e. planets with masses about Jupiter mass or higher), the strong interaction between gas and disk allows the planet to repel gas about its surroundings, creating an annular gap.

The effects of low mass and high mass planets are represented in Fig. 3.2.

In the following subsections we will examine in detail these two cases.

3.2.1 Type 1 migration

As we have just said, Type 1 migration is characterized by low mass planets that little affect disk structure.

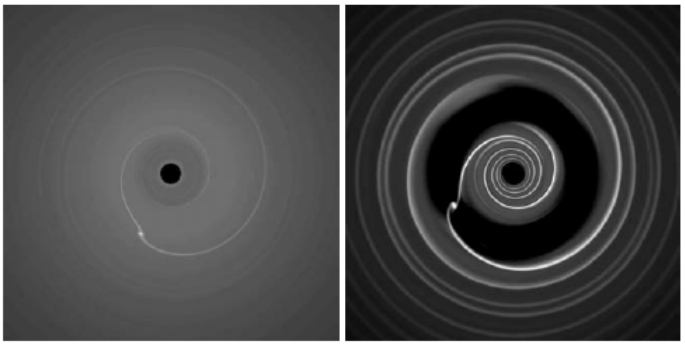

Figure 3.2: *The figure on the left shows a low mass planet orbiting around the star, embedded in the circumstellar disk. Its mass does not allow to open a gap and it will migrate with a Type 1 migration. The figure on the right shows a giant planet, whose mass allows it to open a gap in the disk. Giant planets migrate with a Type 2 migration.* **Credit**: [15]

Since this interaction results in a sum of torques acting on the planet, each of which can be positive or negative, we will have to calculate the total torque in order to predict where the planet will migrate.

Since the main contributions to the torque come from resonances, we can write total torque as

$$\Gamma = \sum_{m=1}^{\infty} \Gamma_{OLR}(m) + \sum_{m=2}^{\infty} \Gamma_{ILR}(m) + \Gamma_{CR} \tag{3.9}$$

where $\Gamma_{OLR}(m)$ are the (negative) torques exerted at outer Lindblad resonances on the planet, $\Gamma_{ILR}(m)$ are the (positive) torques exerted at inner Lindblad resonances and Γ_{CR} is the torque exerted at co-rotation resonance.

From a purely theoretical point of view, the sums of eq. 3.9 extend to infinity. In particular, we see from eq. 3.8 that for $m \to \infty$, Lindblad resonances lies closer to the planet orbital radius.

However, in the vicinity of the planet, the relative flow between gas and planet is subsonic. This implies that no acoustic waves are excited in this region of subsonic flow.

The flow becomes sonic at a distance of about $\frac{2}{3}h$, so the main contributions to the torque will come from resonances at radii

$$r = a \pm \frac{2}{3}h \tag{3.10}$$

In order to have an account of positive and negative torques, one can introduce the parameter

$$f = \frac{\Gamma_{ILR} + \Gamma_{OLR}}{|\Gamma_{ILR}| + |\Gamma_{OLR}|} \tag{3.11}$$

So, if $f < 0$, outer Lindblad resonances would dominate over the inner ones, implying planet inward migration, while if $f > 0$ the opposite would be true.

It is also possible that $f = 0$. In this case there is a substantial balance between positive and negative torques. Here angular momentum is transferred from the inner disk to the outer disk via the planet, which stays in its original orbital radius, without migrating.

It has been proven for several reasonable configurations with low mass planets embedded in the disk that the net Lindblad torque experienced by the planet happens to be always negative, implying inward migration [30].

One may think that, since torque strength depends on gas density, a steeper density profile would reverse the migration direction. But this is not the case.

Indeed, this would imply a steeper pressure profile too. As we have seen, a larger gradient in pressure profile has the consequence of lowering orbital velocity of the gas to sub Keplerian velocities. This would shift outer resonances closer to the planet, enhancing their strength.

An expression for Lindblad torque which accounts for all Lindblad resonances in an isothermal, three dimensional protoplanetary disk has been obtained by Tanaka, Takeuchi and Ward [31]

$$\Gamma_{LR} = -(2.34 - 0.10p)\left(\frac{M_p}{M_*}\right)^2\left(\frac{h}{r}\right)^{-2}\Sigma a^4\Omega_K^2 \tag{3.12}$$

where the negative sign in front of the expression indicates that the planet is migrating inwards and p is the power index for the density profile.

In particular, we note that the torque is proportional to the planet mass through M_p^2 and, as one would expect, to the surface density of the disk.

This leads to an expression for the migration time [29]

$$\tau_{mig} = \frac{r_p}{\left|\frac{\mathrm{d}r_p}{\mathrm{d}t}\right|} = \frac{1}{2}\left(\frac{h}{r}\right)^2\frac{M_p}{q^2\Sigma_p r_p^2}\Omega_p^{-1} \tag{3.13}$$

where we have defined $q = \frac{M_p}{M_*}$.

For an Earth-mass planet in a typical protoplanetary disk we obtain migration times of the order $\tau_{mig} \sim 10^5$ yrs. We can see that these times are shorter than the characteristic disks' lifetimes; this leads to wonder what kind of mechanisms can stop or slow down inward migration.

As we have previouly seen, a contribution to the total torque comes from corotational resonances too. This is due to the interaction between the planet and the gas that is co-orbital with the planet.

Calculations of corotational torque show that it is positive for disk models with $p < 3/2$ and with negative radial entropy gradient. This leads to a slowing down of the inward migration due to Lindblad torque.

Two quantities are relevant in the evaluation of corotational torque: vortensity and entropy gradient.

Vortensity is defined as

$$\omega = \frac{\nabla \times \mathbf{v}}{\Sigma} = \frac{\Omega}{2\Sigma} \tag{3.14}$$

where the last equality is valid for a Keplerian disk.

In ideal disks, vortensity and entropy are conserved on streamlines, so the displacement of gas elements from an orbital radius to another due to the interaction with the planet leads to develop density perturbations in the disk in order to maintain local pressure equilibrium. These perturbations provide a torque on the planet.

As an example of how corotational torque works, we can consider the case of a protoplanetary disk where temperature is decreasing with orbital radius in a steep way.

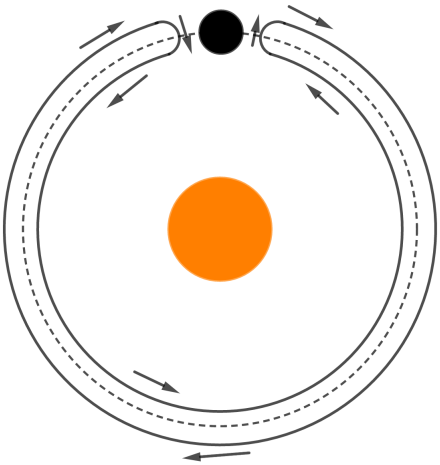

Figure 3.3: *In the planetary reference frame, gas in the inner and outer orbits circulates in opposite directions. When the gas from the outer orbit gets near the planet, the interaction with it causes the gas to be transported to an inner orbit. Since the temperature gradient is steep, this gas element has to contract, forming a higher density region, in order to preserve pressure equilibrium. The opposite is true for inner gas elements transported to outer orbits.*

In the planet reference frame, gas close to its orbit follows horseshoe orbits, with inner gas elements passing to external orbits through the interaction with the planet, and vice versa (3.3).

Now, the displacement of outer gas elements to inner, warmer regions must preserve entropy and pressure equilibrium. This leads the cooler gas to contraction, creating a high density region in front of the planet.

The opposite process, leading to the creation of a low density region behind the planet, occurs for gas elements passing to outer orbits.

This density asymmetry leads to a positive torque on the planet.

Calculations show that corotational torque is too weak to considerably slow down migration due to Lindblad resonances, even if there are certain cases where it has considerable effects on total torque and, consequently, on planet migration [32]:

- The corotation torque can dominate over Lindblad torque when the planet is located at a sharp surface density gradient in a disk, such as the edge of a cavity.

- For Neptune-sized objects corotation torque can even reverse migration due to Lindblad resonances in sufficiently thin disks.

3.2.2 Type 2 migration

We have seen in eq. 3.12 that the torque due to Lindblad resonances scales as M_p^2. So, if the planet mass increases, the presence of the planet can no longer be seen as a simple

perturbation on disk structure. Instead now the presence of the planet affects in a relevant manner the disk structure, leading to the formation of gaps in the gaseous disk.

Gap formation is due to the high transport of angular momentum from the planet to the disk (for gas external to planet's orbit) and from the disk to the planet (for gas internal to planet's orbit). The consequence of this is a mutual repulsion between gas and planet, which translates in the formation of an annular gap.

We have seen that identical processes happened for smaller planets (i.e. type 1 migration), but in that case angular momentum transport was not so intense and viscous forces closed the forming gap.

So, if we want to determine an (approximate) transition regime between type 1 and type 2 migrations (i.e. a planet mass above which we have gap formation), we will have to balance the two competing forces, that are planetary torque and viscosity.

Given a disk with thickness h, the smallest gap a planet could open is $2h$ wide. This because gaps smaller than vertical thickness happen to be unstable.

We can consider a planet at orbital radius a which is opening a gap between $a-h$ and $a+h$. In order to repel all of the gas between a and $a+h$, we have to add an amount of angular momentum ΔJ, given by

$$\Delta J = 2\pi a h \Sigma \left.\frac{\mathrm{d}l}{\mathrm{d}r}\right|_a \cdot h \tag{3.15}$$

where $l = \sqrt{GM_* r}$ is the specific angular momentum of gas in the case this follows a Keplerian orbit.

So, we can define an opening time for the gap

$$t_{open} = \frac{\Delta J}{|dJ/dt|} \tag{3.16}$$

with $|dJ/dt|$ the rate of variation of angular momentum that can be evaluated through the impulse approximation as in [15].

Conversely, we can also define a closure time for the gap, due to viscosity effects

$$t_{close} = \frac{h^2}{\nu} \tag{3.17}$$

and, using α-prescription for the viscosity, we arrive at the definition of a critical planetary mass for the opening of a gap:

$$q_{crit.} \simeq \left(\frac{27\pi}{8}\right)^{1/2} \left(\frac{h}{r}\right)^{5/2} \alpha^{1/2} \tag{3.18}$$

where $q = \frac{M_p}{M_*}$.

The evaluation of this parameter for characteristic protoplanetary disks gives a value $q_{crit.} \simeq 2\times10^{-5}$ that, for planets orbiting around Solar type stars, corresponds to $M_p \simeq 10 M_\oplus$.

At the inner edge of the gap, the planetary torque removes the exact quantity of angular momentum, so that gas cannot invade the gap, counteracting in this way viscous evolution which would tend to fill in the gap.

The same process happens at the outer edge of the gap where, instead, the planetary torque adds an amount of angular momentum to the gas, avoiding in this way that gas fills the gap.

So, there is this continuous exchange of angular momentum between inner and outer edges of the gap, with the planet that works as a mediator.

While the inner edge loses angular momentum, gas flows inward, away from the edge. Since the edge was in a resonant location, where torque is transmitted, the effect of the outer edge is now to push the planet inward, until the inner edge of the gap is placed in its original resonant location, so that the gap is in equilibrium.

Consider a disk whose regions near the planet contain more angular momentum than the planet, that is

$$f \equiv \frac{M_p}{\pi a^2 \Sigma} \leq 1 \tag{3.19}$$

where Σ would be the gas surface density in the region where the planet is located, in absence of the planet.

In this case, we can approximate the planetary migration rate as

$$v = -\frac{3\nu}{2r} = -\frac{3}{2}\alpha \left(\frac{h}{r}\right)^2 v_K \tag{3.20}$$

where we have adopted the α-prescription for viscosity in the last equality.

In particular we note that, differently from type 1 migration, here migration rate is independent on the mass of the planet.

However, this estimate of the migration rate applies only to relatively low mass planets because of the condition 3.19.

Migration rates for planets with $f > 1$ can be determined through numerical simulations, but there is not a general formula, since here the rate strongly depends on viscosity details.

So, the existence of a migration mechanism justifies the presence of giant planets near to their central star (hot Jupiters), allowing them not to form *in situ*, but rather in outer disk regions, from where they subsequently move towards inner regions.

As we have seen for type 1 migration, even for type 2 migration characteristic timescales are of the order of 10^5 yrs. So, planets could reach small orbits around the star in short times but, since the gaseous disk is not yet dissipated, they continue their migration, falling onto the star, unless a mechanism that stops migration acts.

In the case such a mechanism did not exist, only late formed planets could survive until disk dissipation.

So far we have defined a critical planetary mass (or more accurately, a critical parameter q) above which planet undergoes type 2 migration with the formation of a gap in the disk.

However, things are not so clear and type 2 migration appropriately describes only planets for which $q \gg q_{crit.}$.

Instead, for planets with $q \geq q_{crit.}$, migration is not well described by type 1 nor by type 2 migration theories, since in this intermediate regime the physics of the interaction between gas and disk is complicated and one cannot neglect details that are negligible in the two regimes.

Indeed, a planet with a mass of about $10M_\oplus$ orbiting around a Solar-like star, has $q \simeq q_{crit.}$ for typical disk parameters.

So, this planet is too massive to consider its effect on the gaseous disk as a simple perturbation but, at the same time, it is not so massive to completely clean the gap, evacuating all the gas.

The remaining gas into the gap can then give rise to corotational, positive torques, that partially oppose to inward migration.

3.3 Resonant capture

The observations of our Solar System show that the existence of resonances between bodies is not an unusual event. This phenomenon is particularly present in minor bodies (satellites, asteroids and comets).

A resonance occurs when there is a simple numerical relationship between frequencies or periods.

The classical idea of resonance is that between the orbits of two bodies whose periods are commensurable, and this kind of resonance is called orbit-orbit coupling.

But there exist other kinds of resonances, among which the spin-orbit coupling, where the rotational and orbital periods of a single body are commensurable. As an example, this is the case of the Moon, with a 1:1 resonance, or of Mercury, with a 3:2 resonance.

Examples of orbit-orbit resonances in our Solar System are provided by Jupiter and Saturn, that are in a 5:2 near resonance, or by the 3:2 resonance between Neptune and Pluto.

Passing to minor bodies, we can find striking resonances among three Jupiter's satellites, Io, Europa and Ganymede, with Io that is in a 2:1 resonance with Europa, that is in a 2:1 resonance with Ganymede [33].

Widening the look outside the Solar System, it has been found that resonances frequently occur even in extrasolar planetary systems.

From now on, we will focus on orbit-orbit resonances only.

Mathematically, we can express the resonance definition as

$$\frac{T_{in}}{T_{out}} = \frac{p}{p+q} \tag{3.21}$$

where T_{in} (T_{out}) is the period of the inner (outer) body and p and q are two integers.

Using the definition of mean motion

$$n \equiv \frac{2\pi}{T} \tag{3.22}$$

we can rewrite eq. 3.21 as

$$\frac{n_{out}}{n_{in}} = \frac{p}{p+q} \tag{3.23}$$

Now, let us define the angle λ between a reference direction on the orbital plane and the radius vector of a planet, by choosing $t = 0$ as the instant when the two planets are in conjunction and, in this moment, putting $\lambda = 0$.

With the passing of time, the angle will increase

$$\lambda_{in} = n_{in} t \tag{3.24}$$

$$\lambda_{out} = n_{out} t \tag{3.25}$$

and so we can define an angle, called resonant argument

$$\theta = (p+q)\lambda_{out} - p\lambda_{in} \tag{3.26}$$

In general, this angle will range in the interval $[0 : 2\pi]$ but, in the case of an exact resonant configuration (i.e. a configuration where eq. 3.21 is satisfied), the resonant argument will remain zero.

In the case of eccentric orbits, things change a little bit, but we can define an analogous resonant argument as

$$\theta = (p+q)\lambda_{out} - p\lambda_{in} - q\bar{\omega}_{out} \tag{3.27}$$

where $\bar{\omega}_{out}$ is the longitude of pericenter of the outer planet that, using the definitions given in Section 3.1, is defined as $\bar{\omega} = \Omega + \omega$.

Further more, for eccentric orbits $\lambda = M + \bar{\omega}$ is the mean longitude, with $M = n(t - t_{peri})$, where t_{peri} is the instant when the planet passes at the pericenter.

So, we will have a resonant configuration between two bodies if θ librates (i.e. assumes only a restricted range of values around 0 or π).

The analysis of the resonant argument assumes the role of a simple criterion to be verified in order to find a resonant configuration.

The most probable explanation for all these resonances is that of the existence of a resonant capture mechanism.

This mechanism starts with two planets in generic orbits. During the migration stage in the disk, it is possible that the orbits converge, until they reach a resonant configuration.

Once they reach this configuration, the two planets are locked in resonance, thanks to the exchange of angular momentum between them which allows the maintaining of such a configuration.

Chapter 4

Dust distribution in circumstellar disk

This chapter will be devoted to the description of the disk model adopted in the study and to the analysis of the results obtained.

Before of this, we will give a brief account on the numerical algorithm used to perform simulations.

4.1 FARGO algorithm

Protoplanetary disks are very complex structures both from physical and mathematical points of view.

As we have seen, from a physical point of view, circumstellar disks can be treated as fluids and they undergo a lot of processes, such as heating and cooling, photoevaporation, accretion onto the central star and many others that we have analyzed in the previous chapters.

From a mathematical point of view, the treatment of disks as fluids translates into the resolution of a set of hydrodynamical equations, also known as Euler equations:

$$\frac{D\rho}{Dt} + \rho \boldsymbol{\nabla} \cdot \mathbf{v} = 0 \tag{4.1}$$

$$\rho \frac{D\mathbf{v}}{Dt} = -\boldsymbol{\nabla} P - \rho \boldsymbol{\nabla} \Phi \tag{4.2}$$

$$\rho \frac{DE}{Dt} = -P \boldsymbol{\nabla} \cdot \mathbf{v} \tag{4.3}$$

where ρ is the mass density, $\mathbf{v}$ is the fluid velocity, P is the pressure and E is the energy density of the fluid.

The operator D/Dt is the comoving derivative, defined as

$$\frac{D}{Dt} \equiv \frac{\partial}{\partial t} + \mathbf{v} \cdot \nabla \tag{4.4}$$

These partial differential equations (PDEs) express the conservation of mass (eq. 4.1), momenta (eq. 4.2) and total energy (eq. 4.3) and it is possible to find an analytic solution only

in very simple situations. A solution to these equations is usually found through numerical methods.

The set of Euler equations is typically closed with an equation of state for the fluid and with the Poisson equation, to whom the gravitational potential Φ is subjected

$$\nabla^2\Phi = 4\pi G\rho \tag{4.5}$$

As we have seen, a disk is strongly influenced by its central star and other heating/cooling mechanisms, so we have to add to eq. 4.3 terms Q^+ and Q^- which account for heating and cooling respectively.

Further more, disks are not only made by the gaseous component. Indeed, there is also dust, which constitutes the seed for planet formation, and planets, which can perturb gas and dust distributions.

The study of all these constituents translates in a set of various equations to be simultaneously solved with many parameters.

Since this task is analitically impossible, in order to manage this complexity a lot of numerical methods and algorithms have been developed in the years.

So, the physical system is represented by some functions $f(x,t)$ and their derivatives. The issue is that we have a continuous function, constituted by an infinite set of points, that has to be transferred to the finite memory of a computer.

So, we see the need of some discretization method which allows to transform a continuous function in a limited set of points. Obviously, the more the points are (i.e. the higher the resolution is), the more representation of the physical system is accurate.

We can divide all these methods in two groups: grid based methods and gridless methods.

Examples of gridless methods are spectral methods, which represent a function $f(x,t)$ as a superposition of basis functions (e.g. sines and cosines), and smoothed particle hydrodynamics methods, where mass distribution is represented through discrete particles.

Grid-based methods, such as the one used in this work (FARGO), are based on a grid, as their name suggests. The grid is divided into cells, each of which contains informations about a little portion of the system. Functions representing the system are then discretized on this grid through a discretization method, which could be a finite difference, a finite volume or a finite element method.

All these discretization methods convert continuous derivatives into differences between discrete data.

FARGO (Fast Advection in Rotating Gaseous Objects) is a grid based method [34].

The grid is divided in N_s azimuthal sections, with $\Delta\theta = \frac{2\pi}{N_s}$, and N_r radial sections, so that we have $N_r \times N_s$ cells. Grid boundaries are located at R_0 and R_{N_r}.

The following step is the discretization of the continuous functions present in Euler equations.

We locate the quantities in the cells in the following way (Fig. 4.1):

- density, denoted by Σ_{ij}, and internal energy are located in the centre of the cells, with $(i,j) \in [0, N_r - 1] \times [0, N_s - 1]$;
- radial velocity v^r_{ij} is azimuthally centered, and is located at the edge of two cells, at the interface between cells $[i,j]$ and $[i-1,j]$;
- azimuthal velocity v^θ_{ij} is radially centered, and is located at the edge of two cells, at the interface between cells $[i,j-1]$ and $[i,j]$.

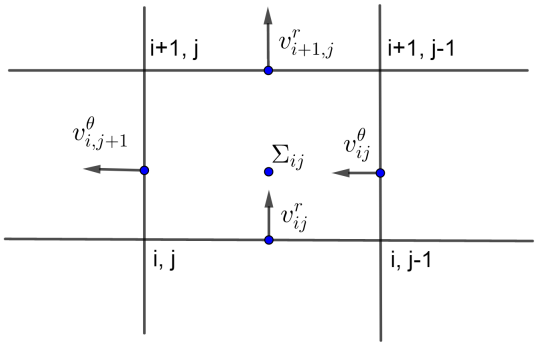

Figure 4.1: *Polar grid is divided into cells, each containing a small portion of the system. Continuous functions are discretized and appropriately located in the grid.*

FARGO's discretization method is a finite difference method, which converts a series of PDEs into a series of algebraic equations.

This method also involves an operator split procedure [35], through which the solution of PDEs is divided into parts, with the output of the first part that constitutes the input for the second part, and so on.

So, if we consider a generic operator $\mathcal{L}(y)$, so that

$$\frac{\partial y}{\partial t} = \mathcal{L}(y) \tag{4.6}$$

and we divide the operator into $\mathcal{L}(y) = \mathcal{L}_1(y) + \mathcal{L}_2(y) + \cdots$, an operator split method allows us to separately solve all these subparts:

$$\frac{y^1 - y^0}{\Delta t} = L_1(y^0) \tag{4.7}$$

$$\frac{y^2 - y^1}{\Delta t} = L_2(y^1) \tag{4.8}$$

$$\frac{y^3 - y^2}{\Delta t} = \cdots \tag{4.9}$$

where L_i is the discretization of the corresponding continuous operator $\mathcal{L}_i$.

As an example, we can consider the operator angular momentum J, which satisfies the partial differential equation in polar coordinates

$$\frac{\partial J}{\partial t} + \frac{1}{r}\frac{\partial (v_\theta J)}{\partial \theta} + \frac{1}{r}\frac{\partial (r v_r J)}{\partial r} = \text{Source terms} \tag{4.10}$$

The addition and subtraction of a same quantity does not change the equation, so we can write

$$\frac{\partial J}{\partial t} + \frac{1}{r}\frac{\partial (v_\theta - \bar{v}_\theta) J}{\partial \theta} + \frac{\bar{v}_\theta}{r}\frac{\partial (v_\theta J)}{\partial \theta} + \frac{1}{r}\frac{\partial (r v_r J)}{\partial r} = \text{Source terms} \tag{4.11}$$

where $\bar{v}_\theta$ is the average azimuthal velocity, which only depends on radius r and time t.

The terms in eq. 4.11 identify the various steps of FARGO algorithm, that are:

- a source step, where HD quantities are updated through the source terms (gravity, pressure, viscosity, $\cdots$);
- a radial transport step, identified by the $\frac{1}{r}\frac{\partial(rv_rJ)}{\partial r}$ term, where the updated HD quantities are transported due to radial flow;
- an azimuthal transport step with velocity $v_\theta - \bar{v}_\theta$, called azimuthal residual velocity, where the updated HD quantities are azimuthally transported due to azimuthal flow with this velocity;
- an additional azimuthal transport step, with average velocity $\bar{v}_\theta$.

Considering ξ to be a generic HD quantity, we can schematically represent these steps as

$$\xi \xrightarrow{S} \xi^a \xrightarrow{R.T.} \xi^b \xrightarrow{A.T.} \xi^c \xrightarrow{A.A.T.(1)} \xi^d \xrightarrow{A.A.T.(2)} \xi^+ \tag{4.12}$$

where S stands for source step, $R.T.$ stands for radial transport step, $A.T.$ stands for azimuthal transport step with residual azimuthal velocity and $A.A.T.$ stands for azimuthal transport step with average azimuthal velocity.

From a mathematical point of view, the previous steps sum up as in the following.

After the source step, we define an average azimuthal velocity at each radius r as

$$\bar{v}_i^\theta = \frac{1}{N_s}\sum_{j=0}^{N_s-1} v_{ij}^\theta \tag{4.13}$$

and, consequently, the residual azimuthal velocity will be

$$v_{ij}^{\theta,res} = v_{ij}^\theta - \bar{v}_i^\theta \tag{4.14}$$

Then, in order to ensure that the material sweeps at most half a cell at each substep, we introduce a shift number n_i, defined as

$$n_i = E\left[\bar{v}_i^\theta \frac{\Delta t}{\Delta y_i}\right] \tag{4.15}$$

where $E[x]$ is the nearest integer to x and $\Delta y_i = \frac{R_i+R_{i+1}}{2}\Delta\theta$.

We write the total velocity at each timestep as

$$v_{ij}^\theta = v_i^{\theta,SH} + v_i^{\theta,cr} + v_{ij}^{\theta,res} \tag{4.16}$$

where

$$v_i^{\theta,cr} = \bar{v}_i^\theta - n_i\frac{\Delta y_i}{\Delta t} \tag{4.17}$$

$$v_i^{\theta,SH} = n_i\frac{\Delta y_i}{\Delta t} \tag{4.18}$$

Now, these last quantities can be better understood with the following example.

Coming back to eq. 4.11, the transport substep with average azimuthal velocity corresponds to

$$\frac{\partial J}{\partial t} + \frac{\bar{v}^\theta}{r}\frac{\partial J}{\partial \theta} = 0 \tag{4.19}$$

and it is possible to prove that

$$J(\theta, t) = J\left(\theta - \frac{\int_0^t \bar{v}^\theta \, dt}{r}, 0\right) \tag{4.20}$$

that is, the solution of the equation at any time t has the same form of the initial profile, except for an azimuthal shift.

So, let us suppose that this shift is 4.7 cells in one timestep. Then, we can decompose this quantity as $4.7 = 5 - 0.3$, where 5 is the nearest integer to 4.7.

Now, the first substep ($v_i^{\theta,cr}$) will shift the material by -0.3 through a classical transport method, while the second one ($v_i^{\theta,SH}$) will simply copy the content of cell j into cell $j + 5$.

Clearly, only the first substep will introduce some numerical diffusion in this last transport step.

So, with reference to the scheme in eq. 4.12, we have the following transported quantities:

$$\xi_{ij}^c = \xi_{ij}^b + \frac{\Delta t}{\Delta y_i}\left(\xi_{ij}^{b,*/v^{\theta,res}} v_{ij}^{\theta,res} - \xi_{ij+1}^{b,*/v^{\theta,res}} v_{ij+1}^{\theta,res}\right) \tag{4.21}$$

$$\xi_{ij}^d = \xi_{ij}^c + \frac{\Delta t v_i^{\theta,cr}}{\Delta y_i}\left(\xi_{ij}^{c,*/v^{\theta,cr}} - \xi_{ij+1}^{c,*/v^{\theta,cr}}\right) \tag{4.22}$$

$$\xi_{ij}^+ = \xi_{ij-n_i}^d \tag{4.23}$$

where in the first and second expressions the operator $*/v^\theta$ depends on the particular numerical transport method and on the velocity field.

The choice of timestep turns out to be an important feature in these algorithms. Indeed, a too large timestep would result in some kind of instability.

In order to avoid this, FARGO applies the Courant-Friedrichs-Lewy (CFL) condition to the timestep, limiting the distance that information can travel in the disk during one timestep.

Since we have various constraints to impose, we sum up CFL condition as

$$\Delta t = \frac{C_0}{\{\max_{ij}\left[\left(\delta t_1^{ij}\right)^{-2} + \left(\delta t_2^{ij}\right)^{-2} + \left(\delta t_3^{ij}\right)^{-2} + \left(\delta t_4^{ij}\right)^{-2} + \left(\delta t_5^{ij}\right)^{-2}\right]^{1/2}\}} \tag{4.24}$$

where C_0 is the Courant number, typically chosen to be $C_0 = 0.5$, and δt_k^{ij}, with $k = 1, \cdots, 5$ are time intervals arising from various conditions that we are going to describe.

Since we want waves in the disk to travel a distance less than one cell at each timestep, we have to require

$$\delta t_1^{ij} = \frac{\min\left(\Delta r_i, \Delta y_i\right)}{c_s} \tag{4.25}$$

where c_s is the sound speed.

Furthermore, we require that particles do not cover distances longer than Δr_i and Δy_i in radial and azimuthal directions respectively. This condition mathematically translates in

$$\delta t_2^{ij} = \frac{\Delta r_i}{v_{ij}^r} \tag{4.26}$$

$$\delta t_3^{ij} = \frac{\Delta y_i}{v_{ij}^{\theta,res}} \tag{4.27}$$

The presence of viscosity in the equations leads to the study of diffusion equations. Computational schemes for this kind of equations require a timestep

$$\delta t_4^{ij} = \min\left(\frac{(\Delta r_i)^2}{4l^2(\Delta v_{ij}^r/\Delta r_i)}, \frac{(\Delta y_i)^2}{4l^2(\Delta v_{ij}^\theta/\Delta y_i)}\right) \tag{4.28}$$

where l is a constant with dimensions of length, describing the strength of viscosity.

Finally, one last condition in order not to disconnect two radially adjacent cells after one timestep states that

$$\delta t_5^{ij} = \frac{1}{2}\left(\frac{v_{ij}^\theta}{\Delta y_i} - \frac{v_{i+1j}^\theta}{\Delta y_{i+1}}\right) \tag{4.29}$$

4.2 Disk setup

We have performed various simulations with different isothermal disk's configurations in order to find one where the two planets were captured in resonance. These did not produce the expected results, at least for the 2:1 and 3:2 resonances. In these cases, the planets did not get into resonance, or their resonant capture lasted very little time, with the two planets that escaped almost immediately.

Passing to adiabatic disk's configurations, we have studied in detail one where the inner planet migrates towards the star, while the outer planet starts with inward migration and then reverses it.

We have studied dust distribution for this particular configuration, finding some interesting features that we will report in the next section. In the following, we will address to this configuration as the first one.

Finally, a configuration where 2:1 resonant capture occurs has been found but, both due to time limitations and to limited computing power, we have not analyzed dust distribution for this configuration. In the following, we will address to this configuration as the second one.

The disk, which surrounds a central star with mass equal to Solar mass, extends between $r_1 = 0.5\,\mathrm{AU}$ and $r_2 = 15.0\,\mathrm{AU}$ and has a profile density

$$\Sigma(r) = \Sigma_0\left(\frac{r}{\mathrm{AU}}\right)^{-p} \tag{4.30}$$

where we have considered $\Sigma_0 = 700\,\mathrm{g/cm^2}$, $p = 1.5$ for the first configuration, while $\Sigma_0 = 720\,\mathrm{g/cm^2}$ and $p = 1.0$ for the second one.

Since we are starting with a disk where planets are already formed, it is reasonable that it has $\Sigma_0 < \Sigma_{MMSN}$.

The disk is computationally modeled through a polar grid, with coordinates (r, θ), with 400×360 cells in the first case and 720×360 cells in the second case.

The disk has an aspect ratio $h/r = 0.02$ for the first configuration, that becomes 0.05 in the second one.

With these parameters the disk has a total mass of about $6 \times 10^{30}\,\mathrm{g}$, which corresponds to $\frac{M_d}{M_*} \simeq 3 \times 10^{-3}$. Since this value makes the Toomre parameter Q defined in eq. 2.11 such that $Q > 1$, we can neglect self gravity in the disk.

Kinematic viscosity is modeled through α-prescription, with $\nu = \alpha c_s h$, where $\alpha = 10^{-3}$, which is a characteristic value for protoplanetary disks.

	Distance [AU]	Mass [$M_\oplus$]	Radius [$R_\oplus$]	Eccentricity
Planet 1	4.0	10	1.6	0.0
Planet 2	6.5	15	1.9	0.0

Table 4.1: Planets' features

The disk is subject to viscous heating and radiative cooling, such that

$$Q^+ \approx \frac{9}{4}\Sigma\nu\Omega^2 \tag{4.31}$$

$$Q^- \approx \frac{32\sigma_R T^4}{3\kappa\Sigma} \tag{4.32}$$

where $\sigma_R = 5.67 \times 10^{-8}\,\frac{W}{m^2K^4}$ and κ is dust opacity.

Two planets, whose features are reported in Table 4.1, are embedded in the disk, orbiting around the star.

These planetary masses correspond to values $q_1 = 3.0 \times 10^{-5}$ and $q_2 = 4.5 \times 10^{-5}$ for the parameter q, defined as $q \equiv \frac{M_p}{M_*}$.

Comparing these values to the critical parameter for the opening of a gap in the disk, whose values result to be $q_{crit} = 5.9 \times 10^{-6}$ for the first configuration and $q_{crit} = 5.8 \times 10^{-5}$ for the second one, we see that we are in an intermediate regime between type 1 and type 2 migration, since $q_i \geq q_{crit}$ in the first case and $q_i \leq q_{crit}$ in the second case, with $i = 1, 2$.

In the first configuration, we have inserted 10^5 dust particles with a radius $s = 1.0\,\mu m$ and 10^5 particles with $s = 1.0\,\text{cm}$.

Particle motion has been integrated by FARGO through N-body methods.

We let the first system evolve until $t \simeq 3 \times 10^4\,\text{yrs}$, while the second (without particles) evolves until $t \simeq 2 \times 10^5\,\text{yrs}$.

4.3 Results

4.3.1 Orbital evolution and gas distribution

The analysis of the evolution of semimajor axes for the two planets (Fig. 4.2) in the first configuration presents a peculiar feature. Indeed, initially both the planets migrate inwards but, while the inner planet continues its inward migration as one would expect, the outer one, at $t \simeq 8\,\text{kyrs}$ reverses the migration direction.

Comparing this to similar disk setups, we can observe that migration reversal seems to depend on disk's gas density.

We performed different simulations with a lower grid resolution where we only changed the initial surface density, taking $\Sigma_0 = 500\,\text{g/cm}^2$ and $\Sigma_0 = 1000\,\text{g/cm}^2$ (Fig. 4.3).

In the lowest density case both the planets reverse their migration more than once. The first time, the planets pass from inward to outward migration at about $t \simeq 6\,\text{kyrs}$. The second time, they reverse migration passing from outward to inward migration. Subsequently, only the outer planet reverses again its migration outwards.

Instead, in the highest density case, both the planets migrate inwards, without reversals, at least until $t = 18\,\text{kyrs}$.

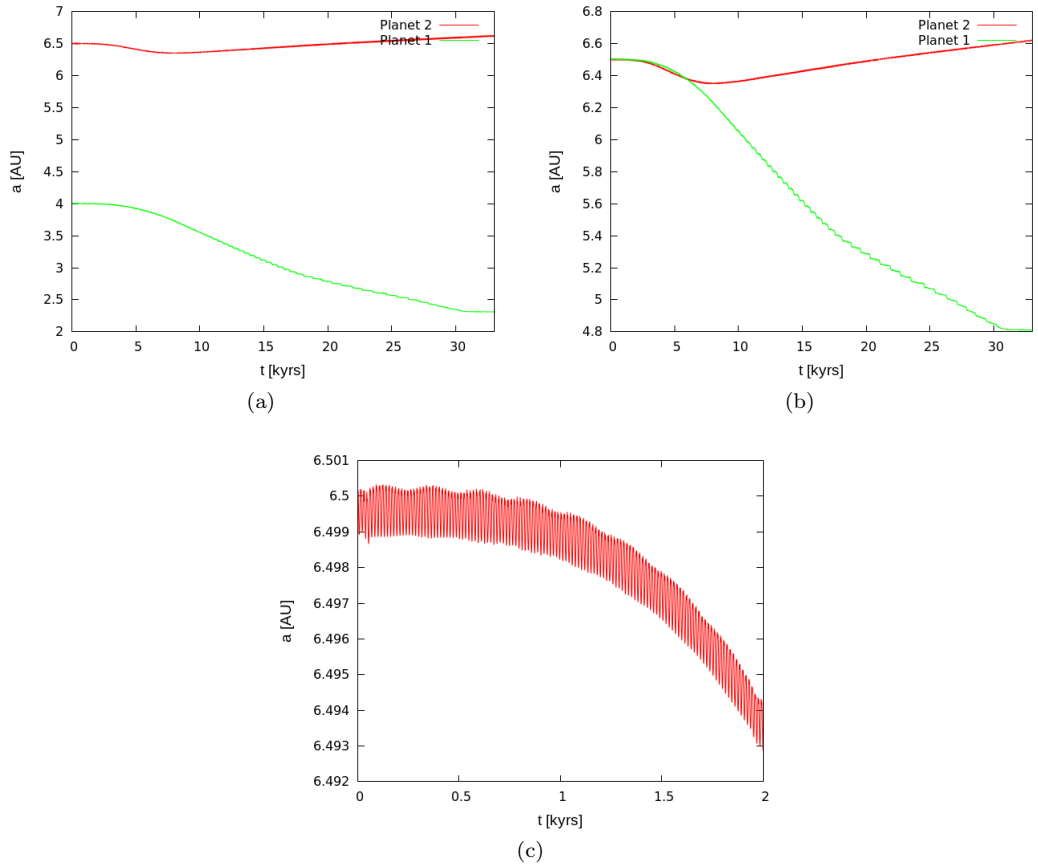

Figure 4.2: *Evolution of semimajor axes for the two planets. While the inner planet always migrates towards the star, the outer planet reverses its migration after* $t \simeq 8\,kyrs$. *In order to better see this peculiar behaviour, the figure on the right vertically shifts the starting point of Planet 1. Bottom figure highlights small perturbations on planetary orbits during migration, due to the interaction between planet and gas density wakes.*

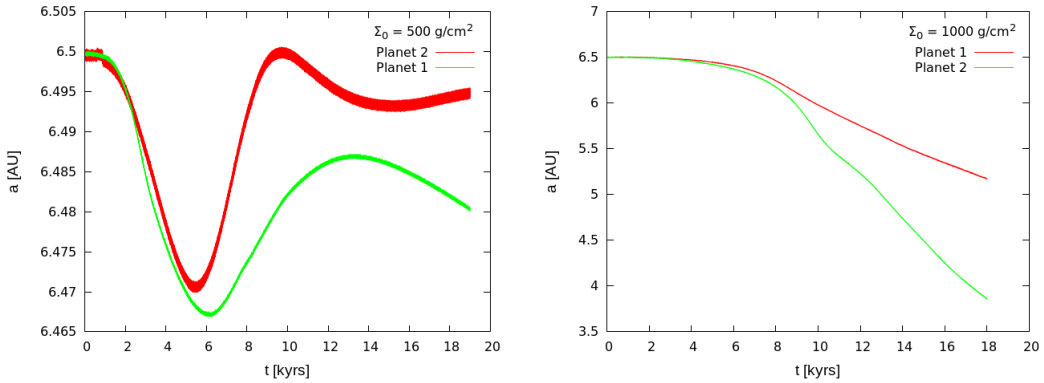

(a) (b)

Figure 4.3: *Evolution of semimajor axes for planets embedded in circumstellar disks with* $\Sigma_0 = 500\, g/cm^2$ *(left figure) and* $\Sigma_0 = 1000\, g/cm^2$ *(right figure). Starting point of Planet 1 has been shifted so as to better enhance the evolution of the orbits.*

In order to understand these features, it is useful to consider the gas density distribution in the disk (Fig. 4.4).

We can observe that the two planets interact with the gaseous disk, giving rise to characteristic wakes. These wakes transport mass and are the cause of the small perturbations in planets migration, displayed in Fig. 4.2. Indeed, wakes interact with planets exchanging a little amount of angular momentum, slightly perturbing their motion. The amplitude of these perturbations is about 10^{-3} AU.

The two planets are opening gaps in gas density distribution, with the most massive planet that is opening a larger and deeper one.

Furthermore, we note that the outer gap is populated by a relatively higher density region, that appears in the radial density profile as a little spike (Fig. 4.5). In this zone, gas is co-orbital with the planet. These regions are known as co-orbital regions or horseshoe orbits.

The presence of horseshoe orbits, whose effect on planetary migration has been described in the previous chapter and in [36], [29], combined with the positive torque on the planet coming from inner Lindblad resonances, could be the cause of migration reversal for the outer planet. Probably, migration reversal does not occur at higher densities because outer Lindblad resonances give rise to a negative torque on the planet that is stronger than the positive one, due to the fact that Lindblad resonances increase with gas density.

However, horseshoe orbit is not stable, and it vanishes at later times.

While the outer planet migrates outwards, the outer edge of the gap shifts in the same direction because of the repulsion of gas due to the exchange of angular momentum with the planet.

Correspondingly, gas from the inner edge shifts outwards too, due to the fact that the outward displacement of the planet produces a smaller repulsive force on the gas.

Indeed, at $t = 8$ kyrs the gap extends from $r \simeq 6.15$ AU to $r \simeq 6.51$ AU, while at $t = 32$ kyrs it extends from $r \simeq 6.41$ AU to $r \simeq 6.75$ AU.

A detailed study of the torques acting on the planet and a comparison with other disk setups could enhance our understanding of the physical processes responsible for the dynamics of the planet.

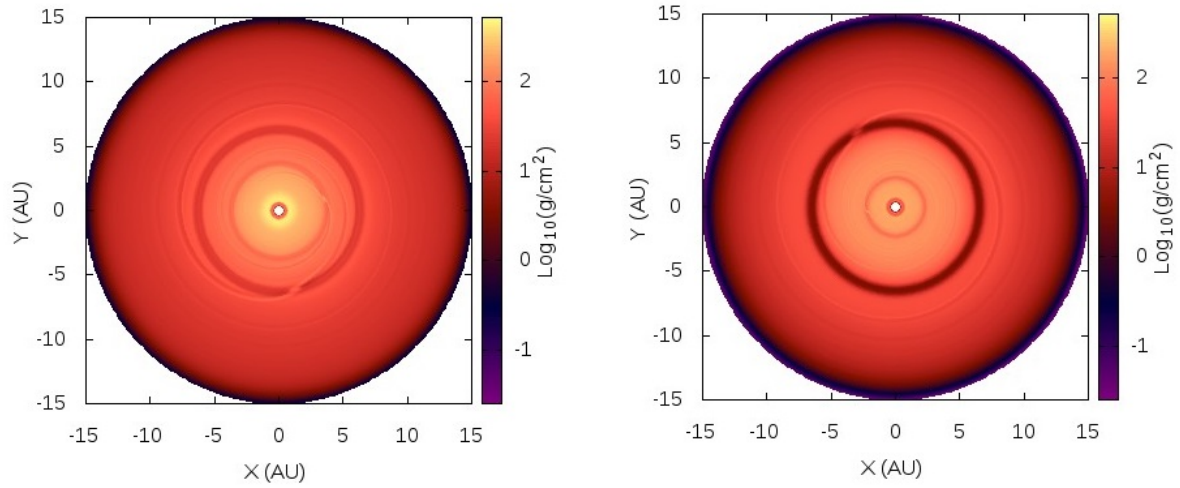

(a) (b)

Figure 4.4: *Gas density distribution at $t = 8\,kyrs$ (left figure) and at $t = 32\,kyrs$ (right figure). Gas density wakes starting from the planets and spiralling throughout the disk can be seen.*

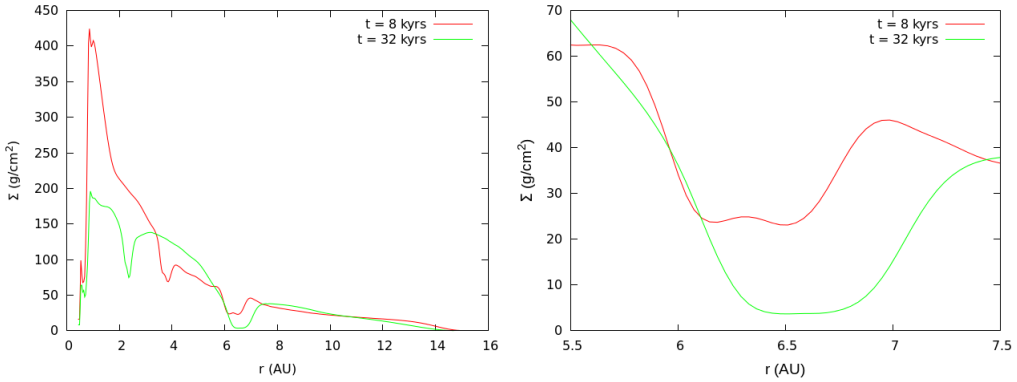

(a) (b)

Figure 4.5: *Azimuthally averaged radial density profile at $t = 8\,kyrs$ (red line) and at $t = 32\,kyrs$ (green line). The gap created by the inner planet starts at about $r = 4\,AU$ and shfits inwards with the planet. The outer gap shifts its edges outwards, following planet migration. The figure on the right highlights the region of the outer gap and the spike in the gap due to the presence of an horseshoe orbit.*

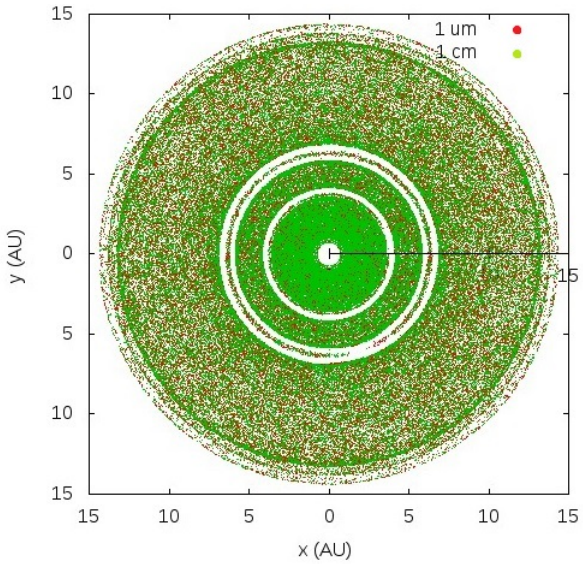

Figure 4.6: *Dust distribution for particles with $s = 1.0\,\mu m$ (red dots) and $s = 1.0\,cm$ (green dots). Two gaps are evident and in the outer one there is a region filled with particles, corresponding to horseshoe orbits (or co-orbital region). It is also shown that no substantial differences are present between the distribution of the two different particles sets.*

Passing to the inner gap, we can see that this is narrower than the outer one, due to the fact that the planet that creates it has a smaller mass. It initially extends from $r = 3.81\,\mathrm{AU}$ to $r = 3.89\,\mathrm{AU}$. When the planet migrates inwards at later times, the gap moves with the planet and the gas fills the regions where the planet previously was.

Considering the limits due to grid resolution, the two gaseous gaps are centered with respect to the planet, that are located at $a_1 = 3.84\,\mathrm{AU}$ and $a_2 = 6.35\,\mathrm{AU}$ respectively.

4.3.2 Dust distribution

We have included in simulations 10^5 dust particles with radius $s = 1.0\,\mu\mathrm{m}$ and 10^5 dust particles with radius $s = 1.0\,\mathrm{cm}$. Particles have density $\rho = 2.65\,\mathrm{g/cm^3}$ and they are uniformally distributed in the whole disk at the beginning.

Temporal evolution of the system leads to the formation of gaps in gas distribution, that translate in the establishment of gaps in dust distribution too. The situation is presented in Fig. 4.6, where both the particles sets are present at $t = 8\,\mathrm{kyrs}$, when the outer planet reverses its migration.

Starting from the disk's outer regions, we can note the presence of three rings where dust particles are concentrated, at 14.3 AU, 13.8 AU and 13.2 AU.

Moving towards inner regions, we observe a substantially uniform distribution down to the outer edge of the gap, where we note a concentration of particles. This is due to the fact that they drift inwards from outer regions of circumstellar disk and stop there, without filtering into the gap.

The gap extends from $r = 5.8\,\mathrm{AU}$ to $r = 6.9\,\mathrm{AU}$ and it would be completely empty if

Disk region	$s = 1.0\,\mu$m	$s = 1.0$ cm
[0.0 : 15.0] AU	98820	98823
[0.0 : 6.1] AU	40386	40383
[6.1 : 6.8] AU	1110	1110
[6.8 : 15.0] AU	57324	57330

Table 4.2: *Particles counting at $t = 8$ kyrs. It can be noted that there is not substantial different temporal evolution between particles with different sizes. First row accounts for all the particles in the disk, second row for particles in the region between the inner edge of the disk and the inner edge of the outer gap, third row for particles in the outer gap and fourth row for particles between the outer edge of the outer gap and the outer edge of the disk.*

there were not horseshoe orbits. The presence of such a relatively higher density region in gas distribution, located at $r = 6.35$ AU, creates a local maximum in radial pressure profile where dust particles are trapped.

A similar pattern repeats moving from the inner edge of the outer gap to the outer edge of the inner gap. Near these edges we find dust concentrations and, in the middle, a uniform distribution of particles.

This gap, narrower than the external one since the planet that creates it is less massive, extends from $r = 3.6$ AU to $r = 4.1$ AU.

Instruments like ALMA can detect this kind of features in circumstellar disks through the observations in dust continuum and spectral line emission [37].

We have calculated Stokes number for dust particles. As we have seen in Chapter 2, this parameter varies with particles' size and with orbital radius. Indeed, we have obtained a value for Stokes number ranging from $St = 10^{-7}$ to $St = 10^{-5}$ for particles with $s = 1.0\,\mu$m and from $St = 10^{-3}$ to $St = 10^{-1}$ for 1.0 cm sized dust.

According to [38] we would expect a different evolution of μm and cm-sized particles, with larger particles that drift inwards faster than smaller particles. Indeed, theoretical models predict an order of magnitude in drift time between particles with $St = 10^{-6}$ and particles with $St = 10^{-2}$.

However, this different evolution is not evident in our simulations, where particles of different sizes have the same dynamical evolution. Table 4.2 presents the counting of particles in various disk regions, highlighting this fact.

This could be due to the fact that dust particles have eccentricities ranging between $0.01 \div 0.09$, with a maximum value of $e = 0.18$. These values are not negligible for small particles and can affect their dynamics. Indeed, theoretical models of dust particle dynamics in disks are based on particles on circular orbits.

Comparison between particles distributions at $t = 8$ kyrs and $t = 32$ kyrs is shown in Fig. 4.7 for μm-sized dust. We have obtained a similar plot for *cm*-sized particles.

Again, starting from the outer disk regions, the analysis of temporal evolution of dust particles distribution shows that the three dust rings, that are now more pronounced, are located at 13.2 AU, 12.3 AU and 11.4 AU respectively. Then, an almost uniform particles distribution follows down to the external edge of the outer gap.

The comparison with the distribution at $t = 8$ kyrs shows that the edge has moved out-

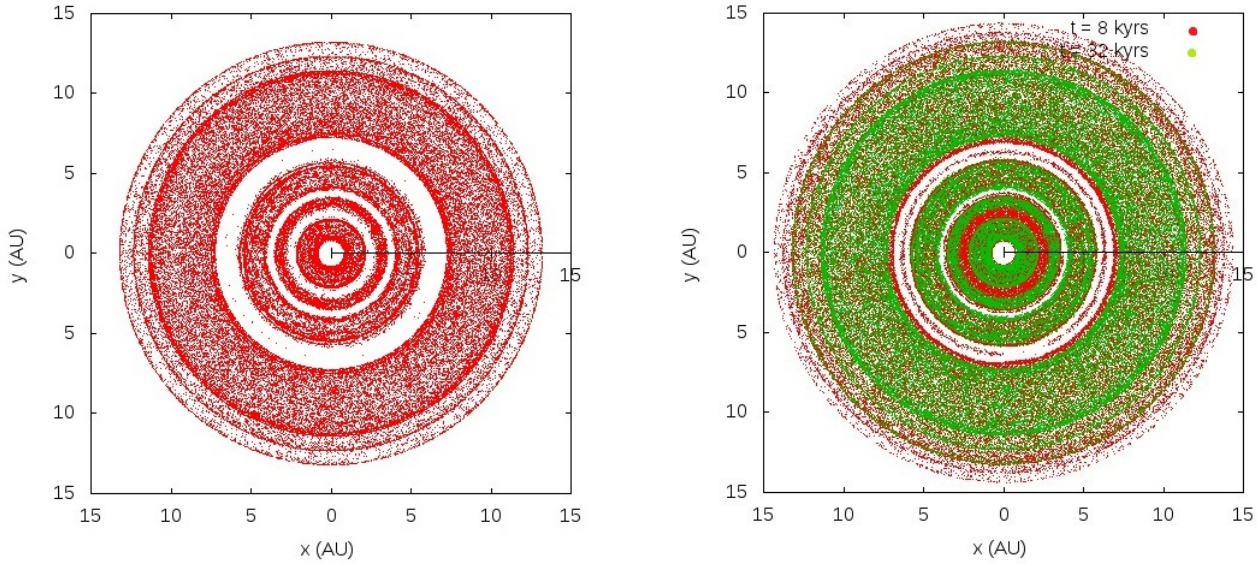

(a) (b)

Figure 4.7: *The figure on the left shows particles distribution at $t = 32$ kyrs. The figure on the right compares dust distributions at $t = 8$ kyrs and $t = 32$ kyrs.*

wards to $r = 7.2$ AU, due to migration reversal of the planet. Instead, the inner edge has not significantly moved outwards. This difference in drift velocity between planet and dust leads to the dust gap broadening.

Furthermore, horseshoe orbits have vanished and particles in it, no more trapped, have drifted towards gap edges.

Moving towards inner zones, we find that the gap previously created by the inner planet between $r = 3.5$ AU and $r = 4.0$ AU has not closed in dust distribution, even if it has been filled with gas.

A possible explanation of this fact can be given considering the resonant capture of edges' dust particles in that zones, combined with the slower drift velocity of dust with respect to planets. Indeed, we see that at $t = 8$ kyrs the ratio between the semimajor axis of the outer planet and that of the outer edge of the inner gap (that at $t = 32$ kyrs becomes the intermediate gap) is 1.55. This value is near to 1.59, that is the ratio of semimajor axes in the case of a $2 : 1$ resonance.

So, when the inner planet migrates towards the star, dust particles of the intermediate edge are trapped in a $2 : 1$ resonance with the outer planet.

At $t = 32$ kyrs the inner planet is orbiting at $a = 2.3$ AU, creating a gap which extends from 2.2 AU to 2.8 AU.

Here, dust gap appears not to be centered with respect to the planet. Again, resonant capture of dust particles and slow particles drift can be invoked in order to explain this fact. Calculating the ratio between the semimajor axis of the outer edge of the inner gap and that of the inner planet, we find that it is about 1.22.

So, particles in this edge appears to be captured in a $4 : 3$ resonance with the inner planet.

Features		$t = 8\,\text{kyrs}$	$t = 32\,\text{kyrs}$
Gaps	Inner	Not present	[2.2 : 2.8] AU
	Intermediate	[3.6 : 4.1] AU	[3.5 : 4.0] AU
	Outer	[5.8 : 6.9] AU	[5.9 : 7.2] AU
Rings	Inner	13.2 AU	11.4 AU
	Intermediate	13.8 AU	12.3 AU
	Outer	14.3 AU	13.2 AU
Planets	Planet 1	3.84 AU	2.32 AU
	Planet 2	6.35 AU	6.59 AU

Table 4.3: *Dust distribution features and planets' positions at $t = 8\,kyrs$ and $t = 32\,kyrs$.*

Dust distribution features are summarised in Table 4.3.

Because of the increasing of gap widths with increasing planet masses, one could think to use this parameter to obtain an estimate of the masses of planets, as done in [39] for giant planets. However, in the case of a circumstellar disk populated by more than one planet, this task can be a little bit more difficult, due to the fact that gap edges feel other planets.

The disk examined in this work is a straightforward case of these difficulties. Here, not only one could estimate a mass that is different from the real one in the case of the inner planet but, observing only dust distribution, one could think that three planets are present.

4.3.3 2:1 resonance

We have tested various configurations in order to find one where the two planets, after a period of convergent migration, are captured into a resonant configuration.

Many setups presented divergent migration, with the inner planet that migrated faster than the outer one or, even, the two planets migrated in different directions.

Some configurations, after a period of convergent migration, reached the resonant capture but this lasted only few years.

This setup is slightly different from the previous one, with $p = 1.0$ instead of $p = 1.5$, where p is the density power index, and a slightly increased density. Furthermore, grid resolution is enhanced.

The two planets start at $a_1 = 4.0\,\text{AU}$ and $a_2 = 6.5\,\text{AU}$, as in the previous configuration.

Fig. 4.8 shows temporal evolution of the two planets' semimajor axes. We can note that the outer planet migrates inwards faster than the inner one until $t = 20\,\text{kyrs}$, when it reverses the migration outwards.

Outward migration lasts for about 40 kyrs, then it comes back to inward migration.

Instead, the inner planet continuously migrates inwards, but slower than the outer planet.

The two planets are captured in resonance after few years of evolution, as shown in the left figure of Fig. 4.9, where the resonant argument θ, defined in 3.27 and calculated with the longitude of pericenter of the inner planet, librates around 0 (and 2π). Right figure shows that at $t \simeq 170\,\text{kyrs}$ planets are in a strong resonant configuration, with the resonant argument calculated with the longiutde of pericenter of the outer planet that starts librating around π, while for earlier times it circulates.

Looking at the bottom plot in Fig. 4.9 we notice that, once the second resonant argument starts librating, the ratio between semimajor axes becomes constant, with a value of $\frac{a_2}{a_1} \simeq 1.59$, characteristic of 2 : 1 resonance.

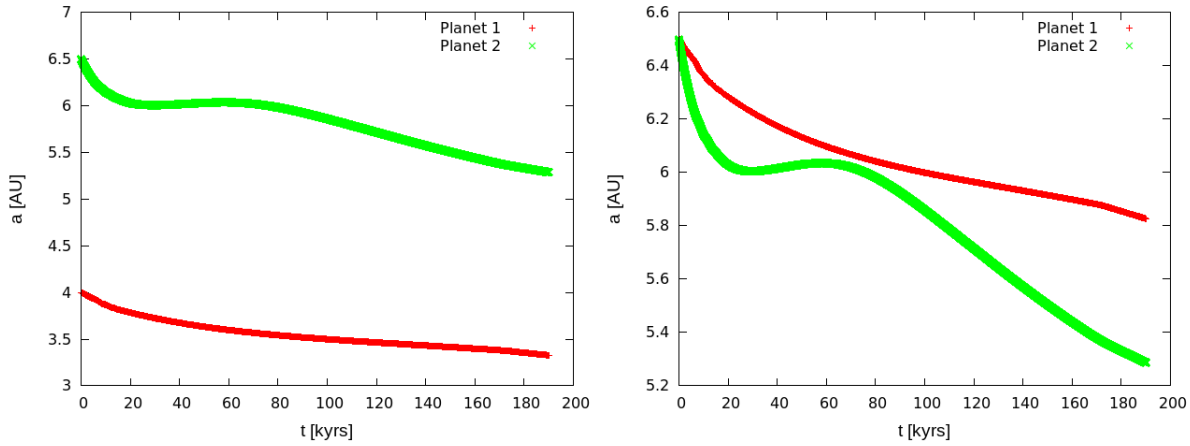

(a) (b)

Figure 4.8: *Temporal evolution of the two planets' semimajor axes. The figure on the right vertically shifts initial semimajor axes so as to enhance the understanding of how semimajor axes evolve.*

Indeed, third Kepler's law states that

$$\frac{a_2}{a_1} = \left(\frac{T_2}{T_1}\right)^{2/3} \tag{4.33}$$

where T is the period of the planet.

In the case of a $2:1$ resonance, we have that $T_2 = 2T_1$ and the ratio in eq. 4.33 assumes the value 1.59.

At this stage, it would be interesting to let the system evolve and to observe if the two planets continue their migration inwards or they reverse it.

The analysis of gas distribution would show if the two planets captured in resonance are able to open a common gap, as in the case of two giant planets [40].

Finally, the addition to the system of dust particles and the successive analysis of the distribution obtained would provide a result that instruments like ALMA could verify.

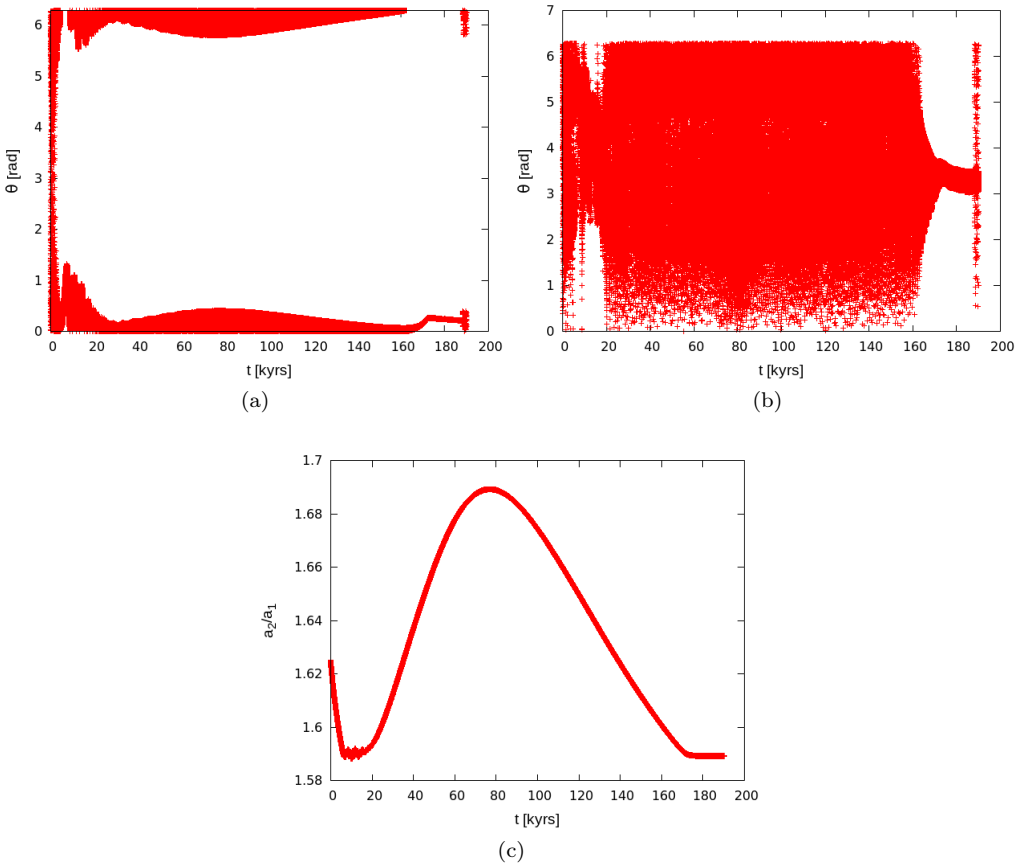

Figure 4.9: *Left figure plots temporal evolution of resonant argument calculated with the longitude of pericenter of the inner planet. When the planets are captured in resonance, this librates around* 0*. Right figure plots the resonant argument calculated using the longitude of pericenter of the outer planet, that librates when the two planets reach a strong resonant capture. Bottom figure plots the ratio* a_2/a_1 *between the two semimajor axes. When the plot becomes constant with time, the planets are captured in a strong* $2:1$ *resonant configuration.*

Chapter 5

Conclusions

In this work we have analyzed gas and dust distributions in a circumstellar disk where, at the beginning, both the planets migrate inwards but, after few thousands of years, the outer one reverses its migration outwards.

The analysis of gas density distribution shows that the two planets open gaps in the disk, with the most massive one that opens a larger gap. When the planets drift, the edges of these gaps follow planet migration and the planet is always centered in the gaseous gap.

The presence of gaseous gaps implies the formation of gaps in dust particles distribution too. Here we have some interesting features, that we will briefly outline:

- Concentrations of dust particles are present, located at the edges of the gaps.
- While the inner planet migrates towards inner regions of the disk, the gap that it had previously opened continues to be open even when gas fills it.

  This fact can be due to the combination of particles' drift velocity that is slower than planet's migration velocity and to the possible presence of some resonant effects between dust and the outer planet that lock particles in that region.
- The presence of possible resonant effects could also explain the fact that the inner gap at $t = 32\,\text{kyrs}$ is not centered with respect to the planet.

  In this case, a $4 : 3$ resonance occurs between particles of the outer edge in the inner gap and the inner planet.
- Theoretical models predict a different evolution for particles with different Stokes numbers. In our case, we do not observe a substantial difference between particles with $St = 10^{-6}$ and particles with $St = 10^{-2}$.

  A possible explanation of this can be due to the fact that particles have not negligible eccentricities that affect their dynamics.

Furthermore, in the outer regions of the disk, we note the presence of three rings where particles tend to concentrate.

All these features can be observed through instruments like ALMA, that detect dust's spectral line emission. The observations of gaps in dust distribution can indicate the presence of sufficiently massive planets in a circumstellar disk, and the measurement of gaps' widths can provide an estimate of planetary masses.

However, as we have seen in our work, the association gap-planet is not so straightforward in disks that contain more than one planet. Indeed, we have observed the presence of an intermediate gap in dust distribution that remains open even if no planets are present into it.

So, a better approach to identifiy the presence of a planet could be the simultaneous study of both the dust and gas gaps. Indeed, in our case, we have seen that even if a dust gap was open, gas filled it, excluding in this way the presence of a planet into it.

Finally, we have analyzed the presence of a $2:1$ resonance between two planets embedded in a disk with slightly different parameters from the previous one.

The presence of such a resonant configuration has been identified through the analysis of resonant arguments and the ratio of planets' semimajor axes.

Possible developments for this work could be the analysis of both gas and dust distribution, in order to verify if the two planets in resonance are massive enough to open a common gap.

Bibliography

[1] P. Bodenheimer, "Historical notes on planet formation", *Planet Formation*, 2006.

[2] T. Birnstiel, "The evolution of gas and dust in protoplanetary accretion disks", 2011.

[3] M. M. Woolfson, "The solar system - its origin and evolution", *Q. J. R. astr. Soc.*, 1993.

[4] NASA. (2019). Exoplanet archive, [Online]. Available: `https://exoplanetarchive.ipac.caltech.edu/`.

[5] A. Wootten, "The atacama large millimeter array (alma)", in *Large ground-based Telescopes*.

[6] J. L. Beuzit *et al.*, "Sphere: the exoplanet imager for the very large telescope", 2019.

[7] M Keppler *et al.*, "Discovery of a planetary-mass companion within the gap of the transition disk around pds 70", *Astronomy & Astrophysics*, 2018.

[8] *Planetary Sciences*. Cambridge University Press, 2001.

[9] M. R. Krumholz, "Notes on star formation", 2016.

[10] J. Bouwman *et al.*, "The formation and evolution of planetary systems: placing our solar system in context", *Planet Formation*, 2006.

[11] H. Klahr *et al.*, "Turbulence in protoplanetary accretion disks: driving mechanisms and role in planet formation", *Planet Formation*, 2006.

[12] M. Clampin *et al.*, "Hst / acs coronagraphic imaging of the circumstellar disk around hd141569a", *Astronomical Journal*, vol. 126, p. 385, 2003.

[13] S. J. Weidenschilling, "The distribution of mass in the planetary system and solar nebula", *Astrophysics and Space Science*, 1977.

[14] C. Hayashi, "Structure of the solar nebula, growth and decay of magnetic fields and effects of magnetic and turbulent viscosities on the nebula", *Progress of Theoretical Physics Supplement*, 1981.

[15] *Astrophysics of Planet Formation*. Cambridge University Press, 2010.

[16] A. Toomre, "On the gravitational stability of a disk of stars", *The Astrophysical Journal*, 1964.

[17] D. Lynden-Bell and J. E. Pringle, "The evolution of viscous discs and the origin of the nebular variables", *Mon. Not. R. Ast. Soc.*, 1974.

[18] N. I. Shakura and R. A. Sunyaev, "Black holes in binary systems. observational appearance", *Astronomy & Astrophysics*, 1973.

[19] P. J. Armitage, "Dynamics of protoplanetary disks", *Annual Review of Astronomy and Astrophysics*, 2011.

[20] D. Hollenbach, D. Johnstone, and H. W. Yorke, "Disk dispersal around young stars", *Protostars and Planets IV*, 2000.

[21] I. Bonnell and P. Kroupa, "Dynamical interactions in dense stellar clusters", 1998.

[22] A. Scally and C. J. Clarke, "Destruction of protoplanetary disks in the orion nebula cluster", *Mon. Not. R. Ast. Soc.*, 2001.

[23] S. Richling, D. Hollenbach, and H. W. Yorke, "Destruction of protoplanetary disks by photoevaporation", *Planet Formation*, 2006.

[24] D. Hollenbach, D. Johnstone, S. Lizano, and F. Shu, "Photoevaporation of disks around massive stars and application to ultracompact hii regions", *The Astrophysical Journal*, 1994.

[25] O. M. Guilera and Z. Sandor, "Giant planet formation at the pressure maxima of protoplanetary disks", *Astronomy & Astrophysics*, 2017.

[26] G. Wurm and J. Blum, "Experiments on planetesimal formation", *Planet Formation*, 2006.

[27] T. Poppe, J. Blum, and T. Henning, "Analogous experiments on the stickiness of micron-sized preplanetary dust", *The Astrophysical Journal*, 2000.

[28] J. Blum and G. Wurm, "Experiments on sticking, restructuring and fragmentation of preplanetary dust aggregates", *Icarus*, 2000.

[29] R. P. Nelson, "Planetary migration in protoplanetary disks", 2018.

[30] W. R. Ward, "Protoplanet migration by nebula tides", *Icarus*, 1997.

[31] H. Tanaka, T. Takeuchi, and W. R. Ward, "Three-dimensional interaction between a planet and an isothermal gaseous disk. i. corotation and lindblad torques and planet migration", *The Astrophysical Journal*, 2002.

[32] F. Masset and W. Kley, "Disk-planet interaction and migration", *Planet Formation*, 2006.

[33] *Solar System Dynamics*. Cambridge University Press, 1999.

[34] F. Masset, "Fargo: a fast eulerian transport algorithm for differentially rotating disks", *Astronomy and Astrophysics Supplement Series*, 2000.

[35] J. M. Stone and M. L. Norman, "Zeus-2d: a radiation magnetohydrodynamics code for astrophysical flows in two space dimensions. i-the hydrodynamic algorithms and tests.", *The Astrophysical Journal Supplement Series*, 1992.

[36] F. Masset, "On the co-orbital corotation torque in a viscous disk and its impact on planetary migration", *The Astrophysical Journal*, 2001.

[37] C. L. Brogan *et al.*, "The 2014 alma long baseline campaign: first results from high angular resolution observations toward the hl tau region", *The Astrophysical Journal Letters*, 2015.

[38] P. J. Armitage, "Physical processes in protoplanetary disks", 2017.

[39] K. D. Kanagawa *et al.*, "Mass constraint for a planet in a protoplanetary disk from the gap width", *Publications of the Astronomical Society of Japan*, 2016.

[40] F. Marzari, G. D'Angelo, and G. Picogna, "Circumstellar dust distribution in systems with two planets in resonance", *The Astronomical Journal*, 2019.